REMOTE SENS. ENVIRON. 31:1–26 (1990)

Vegetation in Deserts: I. A Regional Measure of Abundance from Multispectral Images

Milton O. Smith, Susan L. Ustin, John B. Adams, and Alan R. Gillespie*

*Department of Geological Sciences, University of Washington, Seattle and *Department of Land, Air, and Water Resources, University of California, Davis*

A method was tested in the semiarid Owens Valley, California for measuring sparse vegetation cover using Landsat Thematic Mapper (TM) multispectral images. Although green vegetation has a characteristic reflectance spectrum in the visible and near-infrared, using conventional image-processing methods, it has been difficult to quantify vegetation cover of less than about 40%, owing to the spectral dominance of the background soils and rocks. Thus multispectral images have been of limited use in mapping variations in vegetation cover in arid and semiarid regions. In this study fractions of vegetation, soils, and shading and shadow within the smallest resolution elements (30 × 30 m pixels) of the TM images were computed by applying a mixing model based on laboratory and field reference spectra. Fractions of vegetation were calculated for each pixel in TM images taken in December 1982 and May 1985, and the results were compared with ground transects. Despite spatial variations in background soil, temporal differences in satellite instrument response, and differences in atmospheric and lighting conditions, the fractions of vegetation computed from each image gave a spatially consistent measure of the projected vegetation cover. Results were obtained for a 150-km segment of Owens Valley; they indicate that the method can facilitate mapping and monitoring sparse vegetation cover over large regions covered by satellite images.

INTRODUCTION

This paper is Part I of a two-part study of desert vegetation, focussed on Owens Valley, California (Fig. 1). In Part I we show how remotely sensed measurements can be used to estimate vegetation abundance in semiarid and arid deserts. In Part II (Smith et al., this issue) we analyze how the environmental factors of net radiation, temperature, elevation, precipitation and soil type affect vegetation abundance in a semiarid landscape.

Ecologists now regard the earth as an integrated ecosystem with fluxes of gases and nutrients among soils, water, biota and the atmosphere (e.g., Walter, 1979; Odum, 1983; Greegor, 1986). New awareness of the integration of processes in the biosphere has increased concern for the fragility and stability of biological communities subjected to a variety of both man-induced and natural climatic changes (Waring et al., 1986). Desert communities are especially sensitive to such changes. Increased human demand for water and predicted climatic changes due to increased atmospheric CO_2 have stimulated a need for greater understanding of the ecology of arid lands and the factors that control the abundance and distribution of natural vegetation.

Address correspondence to Dr. Milton O. Smith, Dept. of Geological Sci., AJ-20, Univ. of Washington, Seattle, WA 98195.

Received 17 July 1989; revised 2 February 1990.

0034-4257/90/$3.50

655 Avenue of the Americas, New York, NY 10010

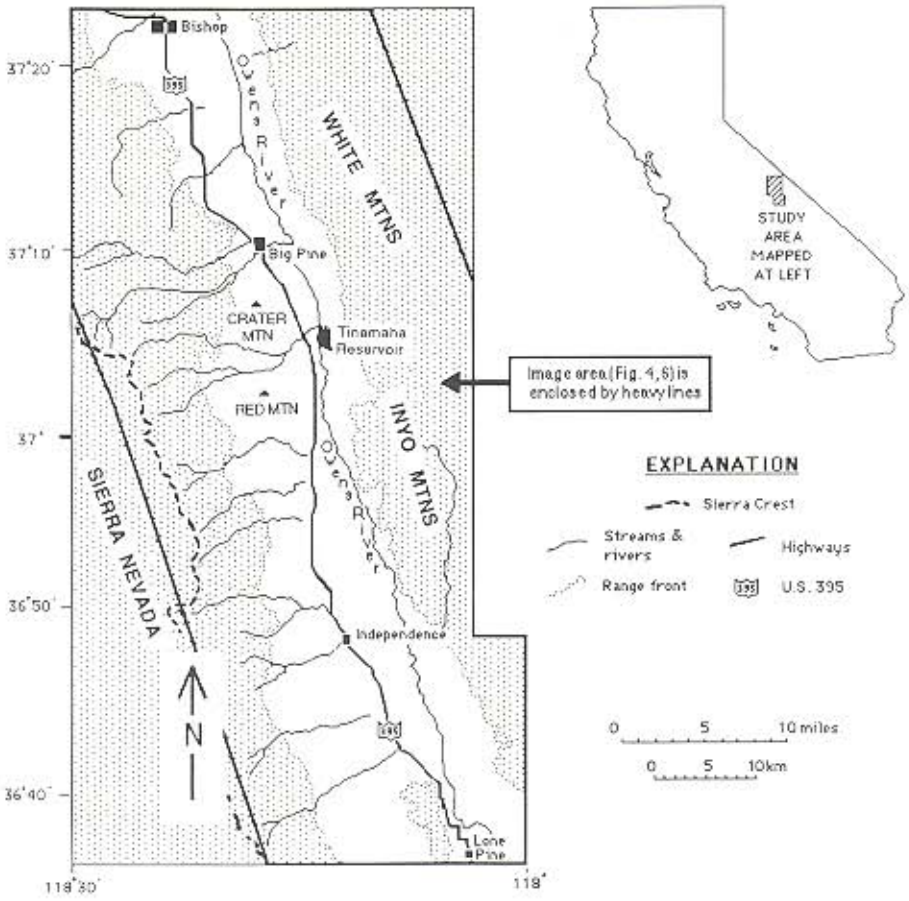

Figure 1. Location of the study area in Owens Valley, California.

Detailed maps of the present-day vegetation in the world's arid lands would facilitate a variety of ecological studies and would provide a reference against which to measure the effects of future changes; however, such information is not generally available. Although extensive field studies of desert vegetation in western North America were made in the past (e.g., Kearney et al., 1914; Shantz and Piemeisel, 1940; Billings, 1945; 1949), such efforts are too expensive and labor-intensive to attempt today. Elsewhere in the world's arid lands there exist few detailed maps of vegetation, because of cost factors and logistical difficulties in conducting ground surveys in remote areas. In the place of extensive field work there presently is an emphasis on modeling of large-scale biophysical processes. Models of ecological phenomena, such as regional desertification, however, still must be validated by ground observations, especially when studying processes of global climatic and land-use changes.

Remote-sensing techniques have the potential to overcome the manpower and fiscal restrictions that now limit large-scale ecological surveys, and recent studies have demonstrated their utility in assessing vegetation distribution (e.g., Justice et al., 1985; Tucker et al., 1985; 1986). Visible and near-infrared multispectral images are the most useful data currently available to examine vegetation patterns and corresponding ecological processes at regional and global scales. Multispectral data are available from earth-observing satellites that date back to 1972, and current satellites provide an expanding data base.

There are two main challenges in applying the vast multispectral image data base to ecological mapping: 1) relating spectral data to the conventional ground-based measurements that are used to characterize vegetation communities, and 2) bridging from the scale of local field measurements to regional and global scales.

1) The first challenge arises because ecologists measuring the properties of vegetation in the field typically do not have to be concerned about reflected solar radiation; however, to make use of remote sensing data it is essential to understand

the correspondence between scene radiance as recorded in multispectral images and field parameters such as vegetation cover, species, community type, and developmental stage. The radiance measured by a multispectral image also is influenced by various factors that are unrelated to the materials on the ground, such as instrumental sensitivity and drift, viewing and illumination geometry, atmospheric backscatter and absorption, and the geometric orientation of surface elements (including topography) within the scene. When these factors have been taken into account, it is possible to interpret the light reflected from a surface in terms of the materials and their mixtures.

2) Satellite images cover spatial scales from tens of meters to hundreds of kilometers. One challenge is to connect observations of vegetation in the field to the measurements made by the smallest resolution elements of the multispectral images (30×30 m in the images used in this study). This requires understanding the reflective properties of the vegetation at the field scale. The next challenge is to extend ecological observations from local areas to larger regions based on the properties measured by the images. If this can be done, the images can become a unique vehicle for exploring regional patterns of vegetation abundance and character, providing new ecological insights.

Remote-Sensing Techniques and the Scale of Observation

There are three main approaches to the problem of estimating vegetation type and abundance from remotely sensed images: 1) the calculation of indices that may be related empirically to the parameters of interest; 2) thematic mapping, or statistical methods of image classification; and 3) spectral mixture analysis. The three approaches share certain strengths and weaknesses in comparison to ground-based investigations. Vast areas of the earth can be surveyed at the same time and in a variety of spectral regions; however, the data depict spectral information only, and the scale of the individual measurement is different from the scale of observation in the field.

The appearance of vegetation varies with the scale of observation. At the large scale of field observations a shrub is seen to consist of different components, including sunlit and shadowed leaves and branches and stems, plus a substrate of litter and soil. These various scene components are characterized by different reflectance spectra. At a smaller scale the shrub components are not spatially resolved, although individual shrubs may be. For example, Figure 2 is a smaller-scale oblique view of a scene of desert scrub in Owens Valley, within our study area. In Figure 2, a single picture element or pixel of $\sim 30 \times 30$ m, typical of Landsat Thematic Mapper (TM) images, has been schematically delineated. This smallest element of a satellite image encompasses shrubs of several species, the shadows cast by shrubs and boulders, shading due to local variations in incidence angle, and the unshadowed soil visible between shrubs. At the small scale of satellite images, components of the individual shrubs—leaves, branches and litter—are not spatially resolved, although they contribute spectrally, even at the subpixel scale. Even at the scale of Figure 2, it is not possible to determine the species of individual shrubs accurately, and this also is true at the scale of most satellite images. The interpretation of the scene may vary with changes in spatial scale, although the materials on the ground remain invariant.

Vegetation indices, reviewed by Jackson (1983), Tueller and Oleson (1989), and others, generally are based on ratios of the radiance in red and infrared spectral bands, chosen to maximize the reflectance contrasts between vegetation and other materials. Some indices have been used to estimate leaf area index (LAI) and other vegetation parameters (e.g., Choudhury, 1988; Elvidge and Lyon, 1985; Huete et al., 1985; Huete, 1986; Tucker, 1979; Jackson, 1983; Kauth and Thomas, 1976). Most commonly used are the vegetation ratio index (VRI), the normalized difference vegetation index (NDVI), and the perpendicular vegetation index (PVI) (Richardson and Wiegand, 1977). Statistical methods of data classification include maximum-likelihood, clustering, and discriminant analysis (e.g., Haralick and Fu, 1983) and methods based on principal-components analysis (e.g., Crist and Cicone, 1984). The objective of image classification is to link image spectra to dominant scene components or to characteristic mixtures of components. It is assumed that spectrally similar data will describe thematically similar elements within a scene. It is also assumed that for each pixel there is a dominant scene component, or at least a unique and identifiable suite of

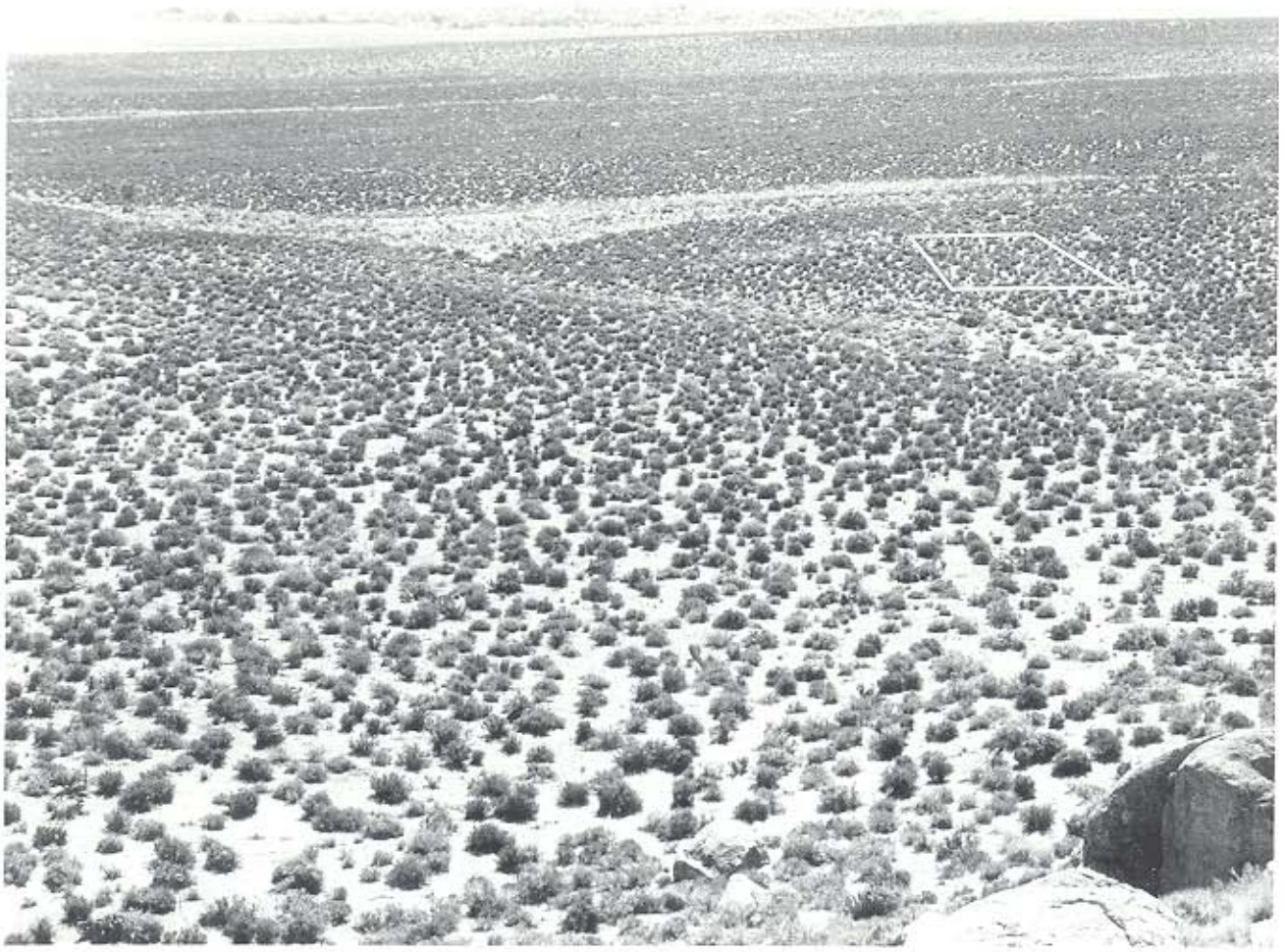

Figure 2. Photograph of desert scrub in Owens Valley. The shrubs themselves are resolvable in the foreground, blurring together in the distance. The outlined figure, roughly a 30×30 m square on the ground, is the area over which light for a single TM pixel is collected. In no pixel is light reflected from a single spectral component of the scene (reference endmember); instead, it is mixed from the soil, the vegetation, and shadows.

components that are present in distinctive proportions.

Vegetation-index and classification techniques have been primarily used to map vegetation in agricultural or forest lands, where the argument can be made that there is a single scene component or class represented in at least some pixels. However, in sparsely vegetated areas this is rarely the case, and index and classification techniques have been shown to perform less well (Ustin et al., 1986a; Tueller and Oleson, 1989; Tucker and Miller, 1977; Huete et al., 1984; Elvidge and Lyon, 1985; Heilman and Boyd, 1986; Huete et al., 1985). In desert scrub environments, for example, thematic classes correspond to characteristic suites or mixtures of components that occur in preferred proportions and at certain illumination geometries (e.g., shaded or sun-facing slopes). The radiance recorded in an image pixel may be mixed from both soil and vegetation, but because soil and vegetation can theoretically mix in any proportion there exists, in theory, an infinite number of classes, even for a scene containing but two components. Clusters of radiance values are thus typically indistinct, and otherwise distinct clusters may overlap because of illumination differences in rugged terrain. Thus rules must be applied to designate thematic classes for many scenes.

Spectral mixture analysis transforms radiance data into fractions of a few dominant endmember spectra which correspond to scene components (Adams and Adams, 1984; Adams et al., 1986; Smith et al., 1985). "Fraction images" depict the mixing proportions of these endmember spectra and thus, via calibration to field data, the mixing proportions of the scene components. Mixture

analysis differs significantly from statistical classification in a number of ways, perhaps most significantly in the small number of endmembers compared to the potentially large number of thematic classes required to describe a scene. Mixture analysis separates the spectral contributions of these intrinsic scene components from shadow and other effects of illumination. This approach is particularly useful for measuring vegetation cover, especially in desert regions where the proportions of vegetation and soil may vary significantly over small distances.

The application of spectral mixture analysis presented in this paper differs from previous discussions of spectral mixing by Horwitz et al. (1975), Jackson (1983), Conel and Alley (1984), Huete et al. (1985), and Pech et al. (1986) in that the approach is directed at using a simple mixture model to link reflectances measured by field and/or laboratory instruments with image relative-radiance measurements acquired by satellite. This is done by referencing to the known spectra of materials and their mixtures on the ground. Although previous studies have discussed the importance of spectral mixtures, they do not provide the methodology to determine the combined atmosphere and instrument calibration at the time of image acquisition, to remove variations in lighting geometry caused by topography and other factors, and to separate spectral mixtures.

In this article we discuss the use of spectral mixture analysis of Landstat Thematic Mapper (TM) multispectral satellite images to estimate vegetation abundance in deserts. In particular, we explore the construction, calibration, and significance of vegetation, soil, and related fraction images of semiarid Owens Valley, California. The method, however, is not limited to any one imaging system, and has been applied to such diverse data as Viking Lander images of Mars (Adams et al., 1986) and the 224-channel Advanced Visible Infrared Imaging Spectrometer (AVIRIS) images of terrestrial scenes (Smith et al., 1988a).

METHODS

The vegetation cover and other maps reported herein were calculated from Landstat TM images using spectral mixture analysis and calibrated by laboratory and field reflectance spectra. The resulting vegetation-fraction images were then further calibrated to percent cover by field measurements of plant community type and cover, together with other ecological parameters. Cluster analysis was used to determine the relationship between radiances and endmember fractions for TM images taken at different times. The cluster analysis also was used to investigate the relationship between conventional remote-sensing vegetation indices and the estimated vegetation fraction. Finally, results were compared to previously published data and maps, where possible. Similarly, soil-fraction images were checked against previous maps.

Site Description

The study area (Fig. 1) consists of a diverse mixture of semiarid vegetation communities and soil types. It is located in Owens Valley, Inyo County, California between the Sierra Nevada to the west and White and Inyo ranges to the east. Owens Valley trends northwest-southeast and is ~150 km long and ~30 km wide. It consists of a central floor of river and lake sediments separating bajadas, which range in elevation from ~1200 to ~1800 m. Permanent streams are found on the Sierra bajada, but only intermittent ones on the eastern fans. Owens River is on the valley floor, which also has numerous small ponds in the wet season. Owens Valley lies within the strong rain shadow of the Sierra Nevada, which rises to 4000 m elevation. The continental climate has cold winters with hot summers, with a precipitation regime dominated by winter storms. Precipitation varies greatly annually and with elevation. The average annual precipitation on the valley floor is ~14 cm, typically with ~77% occurring between November and March (NOAA, 1986; Hollett et al., 1988). Mean January and July temperatures are 2.9°C and 25.0°C, respectively.

Owens Valley is part of a broad ecotone between typical Great Basin and Mojave desert shrub communities to the north and south (MacMahon and Wagner, 1985; Ustin et al., 1986a; West, 1983a, b, c). In eastern California the transition between these two community types occurs within the range of elevations found on the floor of Owens Valley (West, 1983a); 1250 m (northern end) to 1100 m (southern end). Most of the Sierra fan vegetation is a Great Basin sagebrush semi-desert (*Artemisia tridentata*) ecosystem type, or Blackbrush (*Cole-*

ogyne ramosissima) transitional type, while the valley floor is dominated by alkali grasslands (*Distichlis spicata*, *Sporobolus airoides*) and saltbush-shadscale communities (*Atriplex* sp., *Sarcobatus vermiculatus*) [Part II, Fig. 1b)]. The lower Sierran fans and White–Inyo fans support a mixed desert scrub including some Mojave elements (e.g., *Franseria dumosa* and *Grayia spinosa*). Mojave elements (e.g., *Larrea tridentata*) extend further north on the White–Inyo fans than on the Sierra Nevada fans. Vegetation patterns are complex because of topographic patterns, a complex geologic history (Gillespie, 1982), and human disturbance including grazing, wildfires on the fans, abandoned farmland on the valley floor, and recent desertification resulting from removal and diversion of water (Griepentrog and Groeneveld, 1981; Groeneveld et al., 1986a).

Field Measurements

Vegetation

Various vegetation sampling methods were used to quantify vegetation abundance in the field. On the fans, vegetation parameters were recorded every 0.1 m along 42 stratified and randomly placed 50-m line-intercept transects (Ustin et al., 1986b). Canopy heights were obtained from plants selected using the point-center quarter method (two p-q per transect) or from nearest-neighbor measures (six per tansect). Another data set consisted of a matrix of 36 5×5 m subplots, integrated to correspond to 11 30×30 m pixels. Perennial plants (recorded by species), standing litter, and boulders (> 0.2 m in height) were measured for height, longest width, and perpendicular width. Percent cover was visually estimated in each subplot for live cover, litter, light and dark soil, and rock. Various sampling methods were used by different groups of researchers to quantify vegetation abundance in the field. Their field work totaled 5 man-years. Further details are given in Ustin et al. (1986b) and Teensma (1981).

Additional transect data from previous studies on the Sierran fans were used to complement our measurements (Teensma, 1981). On the valley floor, a vegetation map of the 7.5-min Independence quadrangle was used as control for our remotely sensed vegetation estimates (unpublished data on file at the Bureau of Land Management and Inyo County Water District, Bishop, CA). This map was developed using low-altitude aerial photographs to delineate map units. Six or more 30-m line transects per map unit were measured to determine species composition and percentage cover.

Soils

Soils on the Sierra bajada were mapped by Gillespie et al. (1986) using some of the remote sensing techniques described in this paper. Turrin and Gillespie (1986) dated interbedded basalt flows to provide constraints on the soil ages. Other constraints are imposed by stratigraphic relationships with glacial deposits for which ages have been estimated using relative dating techniques (Gillespie, 1982). Conventional studies of soil development profiles and soil chemistry were conducted at Oak Creek, in part to verify the remote-sensing interpretation (Burke et al., 1986). In general, the soils are young (10–25 ka) camborthids and torriorthents, poorly developed on bouldery granitic franglomerate. Better developed and older soils were haplargids colored tan by iron oxides (~ 200 ka). Less common were eroded haplargids (~ 500 ka), weakly cemented by iron oxides.

Valley-bottom soils are being described and mapped by the USDA Soil Conservation Service (SCS) as part of the Benton–Owens Valley Area Soil Survey (unpublished data, SCS, Bishop, CA). A range of soil types was found. Soil development generally reflected the depth to the shallow water table, which was only a few meters or less before the historic groundwater drawdown by Los Angeles. These soils were developed on generally fine-grained river and lake sediments, and are camborthids, torriorthents, and argixerolls. Some (natrargids) are typified by surface encrustations of salts.

Some soils of the arid eastern bajada were described as a part of the SCS survey. Others near Tinemaha Reservoir have been mapped by J. Herrick (unpublished data, 1988). They are typically calcic, even where the parent material was the same as on the Sierran bajada. In addition, a wider range of lithologies was present, dominated by Paleozoic dolomites, quartzites, and other metamorphosed sedimentary rocks. Most of the soils are camborthids, torriorthents, and calciorthents. No haplargids were observed.

simulate = imitate

Spectral Analysis

Total-hemispherical laboratory spectra of field samples were measured using a modified Beckman 2K-DA spectrometer. Bidirectional field spectral measurements were made using the Portable Field Reflectance Spectrometer (Goetz et al., 1975). Conversion between these two types of measurements is discussed by Hapke (1981). All soil types within the scene were sampled. Plant samples of the dominant species were collected at various times during the year. Intact branches were clipped, placed in sealed plastic bags, and refrigerated until analyzed in the laboratory within 1–5 days after collection. We found that no significant spectral changes occurred during this interval. Samples were grouped by species, and for each species they were separated into green (healthy) leaves, woody stems, dry litter, senescent leaves, and flowers and/or fruits.

Thematic Mapper Data

The Landsat Thematic Mapper (TM) data were rectified to geographic coordinates (USGS, 1979). Relative radiance "digital number" (DN) values were converted to bidirectional reflectance by applying a nominal instrument calibration (Robinove, 1982) and by making a nominal atmospheric correction (Otterman et al., 1980). We use the term "nominal" calibration because we later make an additional correction using the combined gains and offsets derived from the mixing model to account for possible instrumental drift and the actual atmospheric parameters at the time of image acquisition. The two TM images used in this study were obtained on 10 December 1982 (Landsat 4, Path 41, Row 35) and 16 May 1985 (Landsat 5, Path 41, Rows 34, 35) at approximately 09:50 PST. The six visible and near-infrared TM bands were used to determine the spectral endmembers and fraction images. Sun elevations at the times of image acquisition were 23° and 59°, respectively.

Spectral Mixture Analysis

Spectral mixture analysis presupposes that different mixtures of a small number of surface materials or components in the scene are responsible for much of the spectral variation in multispectral images, and that these components have different reflectance spectra (Adams et al., 1989). Areal or "checkerboard" mixtures of components in the scene are expressed as linear combinations of their respective spectra in the image [for a discussion of "intimate" or nonlinear mixing see Johnson et al. (1983) and Shipman and Adams (1987)]. Thus, vegetation cover estimates based upon multispectral images require separating the spectral contributions of vegetation and other surface components.

If component mixtures are the major source of spectral variation in the scene, then it is possible to extract a set of spectra from the image such that mixtures of these spectra simulate the actual observations well, or are a "good fit" to the observed image. The set of spectra was identified for each image studied, using a combination of automated factor analysis and visual inspection of the multidimensional data clusters for trends or structures originating from component mixtures. The goodness of fit is measured by the residual spectral variance, which is a measure of the amount of spectral variation *not* predicted by the model. A "good fit" is one for which this variation is at a level characteristic of the instrument noise.

Endmembers

To identify the characteristic endmember spectra that mix to comprise an image, we use factor analysis interactively with trend analysis of the data clusters. We have named the spectra thus identified from the radiance data alone "image endmembers." Image endmembers are themselves expressed as mixtures of spectra of meaningful scene components, defined by the field scientist. We have named these scene components "reference endmembers"; their spectra are named "reference endmember spectra." Both image endmembers and reference endmember spectra will vary with image scale (Fig. 3).

The spectral contribution of endmembers in an image may be quantified, pixel by pixel, as a fractional abundance of each spectral endmember, which generally corresponds in a straightforward way to the abundance of the corresponding scene component. The fraction of any endmember is constrained to lie between 0 and 1, and the sum of the fractions for each pixel is required to equal unity. A fraction of 0 implies there has been no contribution from the particular spectral endmem-

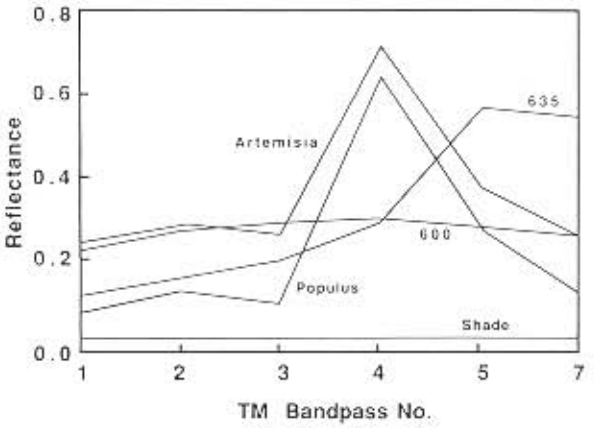

Figure 3. The five reference endmember spectra (two each of vegetation and soils, plus shade) that best fit the image endmembers [Eq. (2)]. These reflectance spectra were measured in the laboratory on a Beckman DK-2A spectrometer and convolved with the six complete TM bandpass transmission spectra to obtain the TM spectra plotted here. The soil spectra were sampled from SCS soil units 600 and 635 ("gray" and "tan" soils, respectively).

ber, whereas a fraction of 1 implies the spectrum for the pixel is identical to the particular endmember. (Fractions outside this range are mathematically possible but physically unreasonable, and suggest that the endmembers were not well chosen.) A more detailed mathematical discussion of image endmembers and mixing is given in Possolo et al. (1990).

Image endmembers are selected such that mixtures of a minimum number of spectra best describe the data; thus they may not correspond to pure materials in the scene, and their identity must be inferred from reference spectra of known materials. For example, an image endmember—like a thematic class in conventional cluster analysis and image classification—might correspond to a mixture of 30% vegetation and 70% soil because no pixels of 100% vegetation or 100% soil are present in the imaged scene. In this example vegetation and soil spectra may themselves be regarded as reference endmember spectra. In practice, reference spectra are typically bidirectional or hemispherical reflectance spectra taken in the field or in the laboratory under controlled conditions using well characterized samples. Bidirectional and hemispherical reflectances are similar for many natural surfaces (Gradie and Veverka, 1982), and thus both may be related to multispectral image data (radiance) via a linear transformation (Hapke, 1981).

Selection of Image Endmembers

The preliminary objective of the study was to determine if each Owens Valley TM image could be represented as a linear mixture of a few distinct spectral endmembers. Image endmembers were selected from image spectra using a set of equations for each band as follows:

$$\mathrm{DN}_b = \sum_{i=1}^{N} F_i \mathrm{DN}_{i,b} + E_b \quad \text{and} \quad \sum_{i=1}^{N} F_i = 1, \quad (1)$$

where DN_b (digital number) is the relative uncalibrated radiance in band b of an image pixel, F_i is the fraction of endmember i, $\mathrm{DN}_{i,b}$ is the relative radiance of endmember i in band b, N is the number of endmembers, and E_b is the error for band b of the fit of N spectral endmembers [see Adams et al. (1986), Possolo et al., (1990), and Smith et al. (1985) for more detailed descriptions of the mathematical procedures]. The maximum number of endmembers (N) is one more than the number of bands. By evaluating Eq. (1) for many pixels, it is possible to make least-squares estimates of the image endmember spectra ($\mathrm{DN}_{i,b}$), and it may turn out that fewer than the maximum possible number of endmembers is required to describe the image adequately.

Equation (1) is used to determine image endmembers by a sequential search of the pixel spectra, requiring that 1) values of F_i for each pixel spectrum computed must lie between 0 and 1 and 2) the least-squares fit to Eq. (1) is "good" [i.e., the root-mean-square (rms) of the E_b values, summed over the number of bands pixels, is comparable in magnitude to the instrument noise]. The atmosphere is considered to be uniform across the imaged area, and its effects are imbedded within the spectral endmembers selected using Eq. (1). If the atmosphere is not uniform across the scene, then it may be necessary to define atmospheric endmembers, or there will be parts of the image that are poorly modeled, as revealed by rms-error or fraction-error images.

For both of the TM images of Owens Valley we calculated an rms term that was < 2 DN levels, or $< 0.8\%$ of the range of DN values in the image. This value is similar to reported values for TM noise [~ 1 DN level: Barker (1983); Anuta et al., (1984)]; thus the image spectral measurements may be described as linear mixtures at the subpixel level. The image endmember spectra provide only relative spectral characterization of the

surface materials, since the image endmembers at this stage of analysis are uncalibrated, and not yet aligned to the reference endmember spectra.

Reference Endmember Spectra

Just as the measured image data may be expressed as linear combinations of image endmembers, so may the image endmembers themselves be expressed as linear combinations of reference endmember spectra. (Reference spectra are reflectance spectra taken by field or laboratory instruments. They are convolved with the TM bandpasses before comparison with the image endmembers.) In this way the imaged scene may be described in terms of its physically meaningful components. The connection between image endmembers and reference endmember spectra consists of 1) a spectral "alignment" of the image endmembers to the reference endmember spectra and 2) a "calibration" relating the image endmembers (nominally calibrated radiance) to the reference endmembers (laboratory reflectance). Thus, the alignment is the linear transformation that defines the image endmembers in terms of mixtures of reference spectra. The calibration also is a linear transform, consisting of a gain and offset for each spectral band. This calibration makes the final correction of the image data to reflectance by adjusting for the combined effects of instrumental drift and atmosphere that were not accounted for in the nominal correction. These operations are described in more detail below.

Aligning image endmembers to reference endmember spectra is a key step in the analysis, as it provides the physical context necessary to interpret the image. Reference endmember spectra are chosen such that when mixed they reproduce the calibrated image endmembers and hence the radiances encoded in the image. Alignment requires that a set of reference endmember spectra be extracted from a larger collection of reference spectra. This set has the same number of spectra as the set of image endmembers.

Selecting Reference Endmember Spectra

The first step in the selection of reference endmember spectra limits the candidate spectra to those that are appropriate to the scene in the experience of the analyst. These candidates are then thematically grouped according to general categories such as "soil" or "bajada vegetation." Then Eq. (2) (see below) is used to calculate mixtures of reference spectra, randomly selected from each general group, necessary to recreate the image endmembers. Inappropriate sets of reference spectra have unrealistic proportions and are rejected. The best few of the remaining sets will be those that recreate the image endmembers, as indicated by their small root-mean-square (rms) residual. Finally, if there is no single best choice at this stage, the reference endmember spectra are subjectively selected from these few survivors based on their physical significance.

The reference endmember spectra are representative of spectra measured in the field. Each may act as a proxy for a number of similar spectra, which could be used in its stead. Selecting one plant species as the best endmember does not necessarily imply that all vegetation in the scene is of this species. On the community level, vegetation may be described by the spectra of whole plants, or by mixtures of plant components such as green leaves, stems, and bark. Although each component itself could be considered as a mixture of even more fundamental spectra (e.g., chlorophyll, cellulose, waxes, water, lignins), this level of biochemical resolution is not necessary to describe the image. A vegetation reference endmember spectrum typically is chosen as a field or laboratory reflectance spectrum of the unshaded foliage of a plant, or as the spectrum of the entire plant, including stems and bark.

Alignment and Calibration

The objective of alignment and calibration is to recognize the most parsimonious solution of system (TM plus insolation and atmospheric scattering and absorption) gains, offsets, realistic endmember fractions, and fit between the image and reference spectral endmembers. Nominal TM sensor gains and offsets, together with the standard solar spectrum and an atmospheric model (Otterman et al., 1980) were used to reject unrealistic solutions (e.g., solutions requiring calibration gains and offsets outside the range of uncertainties). For the purpose of discussion, we may regard alignment and calibration as separate processes, but in practice they are performed simultaneously. The first conceptual step is "aligning" the image endmembers to the reference endmembers. The second step is calibration of image spectra from encoded radiance values to reflectance. The

two steps are carried out by solving for fractions F_r, gains G_b, and offsets O_b using the following equation:

$$G_b \mathrm{DN}_{i,b} + O_b = \sum_{r=1}^{N} F_r R_{r,b} + E_b \quad \text{and} \quad \sum_{r=1}^{N} F_r = 1, \tag{2}$$

where $R_{r,b}$ is the laboratory or field reflectance in band b for reference endmember r, and $\mathrm{DN}_{i,b}$ is the uncalibrated radiance in band b for image endmember i. Note that values of E_b and F_r need not be the same as those for the equivalent terms in Eq. (1). Equation (2) is applied to the set of image endmembers and reference endmember spectra, and not to the image data as in Eq. (1), but the calibration coefficients G_b and O_b are applicable to the image data, and are treated as constants for a given image. Embedded within the calibration coefficients are multiple effects of the instrumentation, the atmosphere, and the illumination intensity, which, to first order, typically are linear. Departures from linearity usually are expressed by a lack of fit to Eq. (2). Variable atmospheric effects over the scene would require the use of additional endmembers.

The reference endmembers themselves are selected in a manner outlined above and analogous to the way in which image endmembers were chosen. This selection involves the repeated application of Eq. (2) for different candidate groups of reference spectra.

Images of Endmember Fractions

Fractions of each reference endmember spectrum can be computed for each pixel of an image. A fraction image for each endmember is thus constructed. Displayed on an image monitor, areas of high fractions will be brighter than areas of low fractions. For Owens Valley, we anticipated, based on field observations, that there would be one or two vegetation endmembers, two or three soil endmembers, and a "shade" endmember which is necessary to relate the image to the other reference spectra.

The shade endmember accounts for shading (variations in lightness due to local incidence angle) and shadows at all spatial scales. At the subpixel scale, where shadows cannot be spatially resolved, it is not possible to tell whether shade is due to shading, shadows, or to a combination of both. We define reference "shade" as the reflectance of an ideal black surface. In images, radiance from shadowed areas contains contributions of light scattered from adjacent terrain and from the atmosphere.

Because $\Sigma F_r = 1$, the fraction images giving the relative abundances of vegetation and soil will be somewhat anticorrelated with the shade fraction (F_{shade}) image, which primarily depicts lighting and topography. It is desirable to normalize the endmembers corresponding to the material components of the scene by rescaling all fractions except F_{shade} such that they sum to unity, pixel by pixel. This procedure removes only the shade fraction from images. As an example, if there were a single vegetation endmember, we may calculate a scaled vegetation fraction (VF_s) from the vegetation fraction (F_{veg}) and F_{shade} as

$$\mathrm{VF}_s = F_{\mathrm{veg}} / (1 - F_{\mathrm{shade}}). \tag{3}$$

In the process of rescaling, it is assumed that shade is equally partitioned among the other endmembers. This asumption is warranted when the shade fraction is contributed by shading (rather than shadows) if the subpixel topography affects all materials more or less equally. For pixels in which the shade component consists primarily of subpixel shadows, equal partitioning may not be correct. If some endmembers are more obscured by shadows than others, rescaling will produce incorrect fractions. There did not appear to be strong partitioning of shadows between vegetation and soil in the bajada areas, where the shrubs had an open architecture.

Unlike F_{veg}, VF_s is a measure of the fractional abundance of vegetation independent of the degree of shadowing or surface topography. A picture of VF_s alone may appear "flat" and may be difficult to relate to topographic features in the scene. In order to facilitate visual inspection, we combine VF_s with the complement of the shade fraction image ($1 - F_{\mathrm{shade}}$) to form a single image for display. The complemented shade image itself illustrates shade fractions in a form that is intuitive (e.g., high shade fractions appear dark rather than light). The VF_s and ($1 - F_{\mathrm{shade}}$) images are combined such that shade and shadow are represented by intensity and ranges of VF_s are represented by colors in the displayed picture. In this combined image the relationships between VF_s and F_{shade} are made explicit by encoding the different frac-

F_r is get from equation (2), and then is normalized for excluding both shade and vegetation.

tions as different perceptual variables (i.e., hue and intensity). In contrast, the single parameter F_{veg} contains much of the same information as VF_s and F_{shade}, but the information is not separate and must be displayed as a single perceptual variable (e.g., intensity).

In calculating VF_s the vegetation fraction is normalized for the amount of shade alone. If there are two or more endmembers that are closely related (e.g., different soils) it may be desirable to normalize the fraction images for not only shade but also for all the other unrelated endmember fractions. Thus it is possible to produce scaled soil-fraction images that discount both F_{veg} and F_{shade} such that the relative proportions of different soil types are displayed. For instance, given two soil endmembers Sa and Sb, a scaled soil fraction for endmember Sa, SaF_s, can be calculated by

$$SaF_s = F_{Sa}/(F_{Sa} + F_{Sb}). \quad (4)$$

Higher values of SaF_s indicate more soil of type a, whereas low fractions correspond to more soil of type b. By excluding both the fractions of vegetation and shade, we obtain normalized fractions of Sa independent of both the topography and vegetation. We may use Eqs. (3) and (4) to compute quantitative fraction images for the reference endmembers that correspond more closely than the original ones to parameters measured in the field. Equation (4) requires that the other endmembers be equally partitioned between Sa and Sb. Field observations (Ustin et al., 1986b; Teensma, 1981) support this assumption.

Cluster Analysis

The biomedical statistics program BMDP1M (Dixon et al., 1979) was utilized to evaluate 1) the temporal stability and internal consistence of the measured radiances and calculated endmember fractions for each TM image, acquired at different seasons and years, and 2) the performance of our spectral measure of vegetation abundance compared to other vegetation indices used in remote-sensing studies. The BMDP1M program groups the input variables using the absolute correlation matrix as a measure of distance. Variables with high correlations are grouped together while variables with low correlations are separated. The number of groups and their degree of separation provide a general indication of the number of factors in the measured and computed variables.

Cluster analysis is a means of testing whether spectral mixture analysis provides a consistent framework with which to evaluate temporal changes in a scene. Such a framework may be obscure in the acquired data themselves, because other temporal changes due to extrinsic factors such as illumination geometry, atmosphere, and instrumentation have not been removed. Because the measured radiance images include such extrinsic factors, it is likely that images from different times are uncorrelated, and this should be revealed by the cluster analysis. It is also likely that "contamination" of measures of vegetation from extrinsic factors will be similarly revealed.

Cluster analysis was performed on a subset of the TM image data that included the ranges of soil, vegetation, and shade found on the bajadas and valley floor. The subset of the scene extended from the Alabama Hills 20 km north to Oak Creek, near the town of Independence. The distribution (histogram) of each variable was continuous and unimodal. The December soil fraction images were filtered using a 5×5 uniform-weight kernel to suppress effects of instrument noise. The filtering was necessary because of the low TM signal/noise ratios at the low winter illumination levels, coupled with the intrinsically low spectral contrast between the two soil endmembers. The solar elevation angle for the December TM image was 23° compared to 59° for the May image, corresponding to more than a twofold decrease in insolation for the December image.

RESULTS

A total of five image endmembers was identified using the method described above. Inspection of the distribution of these image endmembers showed that only four of them were required to describe the bajadas; the fifth was found only in riparian areas. We therefore considered the bajada and riparian areas separately. All five image endmembers for each image (em_{D1-5} and em_{M1-5} for the December and May images, respectively) are given in Table 1; em_{D1-4} and em_{M1-4} are the image emdmembers that pertain to the bajadas.

For both the December and May TM images we aligned and calibrated the four image end-

Table 1. Image Endmembers, Calibration Gains and Offsets, and Reference Spectra for Owens Valley[a]

	TM_1	TM_2	TM_3	TM_4	TM_5	TM_7
Image endmembers (DN units)	from pure pixel					
em_{D1}	75.7	31.2	40.5	41.8	65.4	33.3
em_{D2}	75.7	31.9	41.4	36.2	52.4	31.3
em_{D3}	115.6	60.4	89.1	84.3	169.5	97.5
em_{D4}	58.5	21.2	21.6	13.4	11.0	6.2
em_{D5}	66.2	28.3	36.4	58.0	68.4	24.3
em_{M1}	138.1	59.3	85.1	97.0	116.4	104.2
em_{M2}	150.0	70.7	113.7	111.6	108.6	104.2
em_{M3}	162.0	65.0	92.2	97.0	100.8	104.2
em_{M4}	186.2	99.3	149.7	150.9	202.9	152.7
em_{M5}	95.7	40.7	38.0	154.7	70.7	28.3
Calibration coefficients						
Gains $\times 10^3$ (Dec.)	2.67	5.39	4.29	6.36	3.91	6.05
Offsets (Dec.)	−0.15	−0.11	−0.09	−0.07	−0.04	−0.04
Gains $\times 10^3$ (May)	1.31	2.76	2.20	3.20	2.00	3.08
Offsets (May)	−0.13	−0.09	−0.08	−0.07	−0.03	−0.03
Reference spectra (reflectance units)						
"Tan" soil	0.11	0.15	0.20	0.29	0.57	0.55
"Gray" soil	0.22	0.27	0.29	0.30	0.28	0.26
Artemisia	0.24	0.28	0.26	0.74	0.38	0.24
Shade	0.00	0.00	0.00	0.00	0.00	0.00
Populus	0.07	0.12	0.09	0.62	0.28	0.12
Coleogyne	0.09	0.11	0.13	0.33	0.23	0.14
Larrea	0.05	0.08	0.07	0.46	0.22	0.10
Dry grass	0.22	0.30	0.35	0.41	0.54	0.41
Plant litter	0.24	0.31	0.37	0.49	0.57	0.45
Salt	0.64	0.71	0.74	0.77	0.59	0.43
Sand	0.28	0.41	0.49	0.55	0.68	0.60
Red basalt	0.05	0.15	0.32	0.36	0.55	0.51

[a]Image endmembers em_{D1-5} refer to the December 1982 TM image; em_{M1-5} refer to the May 1985 image. Image endmembers are given in DNs (encoded radiance) and must be calibrated using the gains and offsets to relate them to the reference spectra, in reflectance units. Image endmembers em_{D1-4} and em_{M1-4} pertain to the bajadas. The reference endmember spectra for the bajada are the first four listed ("tan" and "gray" soil, *Artemisia*, and shade). *Populus* was the fifth reference endmember, and pertained only to riparian areas. The remaining reference spectra are found in the scene but were not the best choices for endmembers.

Table 2. Alignment between Image Endmembers and Reference Endmember Spectra for the Sierra Nevada Bajadas, for TM Images from December 1982 and May 1985[a]

Image Endmember	*Reference Endmember*				*Fit, rms Error*
	"Tan" Soil	*"Gray" Soil*	*Artemisia*	*Shade*	
December					
em_{D1}	0.29	−0.09	0.18	0.63	0.004
em_{D2}	0.21	0.05	0.10	0.65	0.002
em_{D3}	0.88	0.16	0.21	−0.25	0.007
em_{D4}	−0.01	0.02	0.00	1.00	0.001
May					
em_{M1}	0.39	0.02	0.09	0.50	0.007
em_{M2}	0.27	0.22	0.11	0.39	0.011
em_{M3}	0.30	0.19	0.05	0.46	0.010
em_{M4}	0.50	0.30	0.17	0.03	0.009

[a]The reference endmembers were "tan" and "gray" soils (SCS 635 and 600, respectively), a vegetation spectrum (*Artemisia*), and shade. The fit (in reflectance) expresses how well mixtures of reference spectra fit the image endmember spectra. Fits among all endmembers are < 1.1% rms reflectance.

Table 3. Proportions of Reference Spectra Necessary to Represent Spectrally Scene Components in TM Images

Scene Component	*Reference Endmember*				*Fit, rms Error*
	"Tan" Soil	*"Gray" Soil*	*Artemisia*	*Shade*	
Populus	0.13	−0.85	1.13	0.59	0.017
Coleogyne	0.11	−0.39	0.72	0.55	0.003
Larrea	0.12	−0.77	1.00	0.64	0.009
Dry grass	0.43	0.79	0.08	−0.29	0.011
Plant litter	0.46	0.72	0.19	−0.37	0.009
Salt	−0.55	2.92	0.10	−1.47	0.014
Sand	0.58	1.12	0.07	−0.77	0.024
Red basalt	0.87	0.09	0.09	−0.05	0.057

members for the bajada to our collection of reference spectra. A number of pertinent reference spectra are given in Table 1, including the ones ultimately selected as the reference endmember spectra. The four reference endmembers for the bajadas were two soils ("tan" and "gray"), vegetation (*Artemisia*), and shade (Tables 2 and 3). They were selected from over 100 candidates by the criteria that 1) their spectra have a "good fit" (small rms error) to image endmembers, 2) the alignment fractions are between 0 and 1, 3) the fractions are realistic based on independent knowledge of the surface materials, and 4) the system gains G_b and offsets O_b necessary for calibration are within the uncertainties of known engineering calibration data and atmospheric models.

The alignments of the four bajada image endmembers to the selected reference endmember spectra are given in Table 2. These alignments are fractions of the reference spectra necessary to recreate the image endmembers. For example, December image endmember em_{D2} is spectrally equivalent to a mixture of 21% "tan" soil, 5% "gray" soil, 10% *Artemisia*, and 65% shade. The same scene imaged at a different time may have different lighting and atmospheric conditions, as well as different instrument calibration coefficients, and the equivalent image endmembers may differ accordingly. Thus May image endmember em_{M2} is fit by the same reference spectra, but in different proportions: 27%, 22%, 11% and 39%, respectively. Image endmembers are defined in the data (DN) n-space, not geographically; a given pixel imaged at different times will have consistent reference endmember proportions, except for shade and vegetation.

In general, sets of image endmembers for images of the same scene taken under different conditions need not correspond to each other; in particular, their alignments to the same reference spectra may differ. We found that for the December and May images, two of the four image endmembers (em_{D1}, em_{M1}; and em_{D2}, em_{M2}) did align similarly with the reference endmembers. The others, em_{D3}, em_{M3}; and em_{D4}, em_{M4}, aligned differently.

All alignment fractions for the May image are between 0 and 1 (Table 2), indicating that they are physically realistic in that their spectral mixtures could create the observed image measurements. Field observations of soils and measurements of vegetation cover and type verified that the image-endmember pixels contained the reference endmembers in the appropriate proportions.

Three of the alignment fractions for the December image were negative (Table 2). The range of uncertainty of the calculated fractions depends upon the spectral contrast of the reference endmembers and the precision of measured radiances. For all six bands, the average rms uncertainty in reflectance between the TM and the laboratory and field spectrometers is 2%. At this level, two of the three negative fractions fall within the range of uncertainty: both the −0.01 fraction ("tan" soil; em_{D4}) and the −0.09 fraction ("gray" soil; em_{D1}) could actually be positive. Thus we dismiss these two small negative fractions as being within the rms error of the measurements.

The negative fraction of −0.25 shade for em_{D3} is too large to be explained by instrument noise. It is best explained if the absolute calibration between the two TM images is in error by a single gain factor. By multiplying the different values of

G_d determined from Eq. (2) for each band by a constant value, we change only the fraction of shade relative to the other endmembers. However, this does not change the relative magnitude of fractions among the other endmembers.

A separate alignment of image endmembers was conducted for the riparian areas and valley floor. This resulted in the selection of *Populus* as a fifth reference endmember. Thus after alignment and calibration, both the December and May TM image measurements could be explained as mixtures of the same set of only five reference endmembers: two vegetation spectra, two soil spectra ("gray" and "tan"), and a shade spectrum (Fig. 3). The vegetation spectra—*Artemisia* and *Populus*—characterized the bajada and riparian areas, respectively. No effort was made to model the snow-covered Sierra Nevada, which would have required a different set of endmembers. The primary difference between the two images of Owens Valley taken at different seasons was in the amounts of shade, F_{shade}, due largely to the different sun elevation angles.

Reference Endmembers

Fraction Images

For each TM image we computed a fraction image corresponding to each of the five reference endmembers shown in Figure 3. Because *Artemisia* and *Populus* did not occur together, we summed the two vegetation fraction images to obtain an image depicting a single measure of overall vegetation abundance, applicable to both the bajadas and riparian areas. Thus only four reference endmember fraction images, shown in Figure 4, are required.

Each fraction image exhibits markedly different spatial patterns. For example, primary patterns in the complemented shade image [Fig. 4a)] correspond to large-scale topographic features and surface albedo. Secondary shade patterns correspond to subpixel-scale topography, surface roughness, and vegetation community and canopy architecture. In contrast to shade, the spatial distributions of the combined bajada and riparian vegetation [Fig. 4b)] delineate sharp boundaries along riparian zones and around moist areas on the valley floor, whereas low and continuous vegetation gradients parallel the east–west elevation gradients on the bajadas. The soil fraction images [Figs. 4c), d)] contain spatial patterns on the bajadas that delineate individual fans. The delineated units radiate from the mouths of creeks at the range fronts, in accordance with known depositional patterns, and in contrast to the patterns of vegetation cover. On the bajada, the two soil types demarcate fans according to age (the "tan" soils are more developed and older). On the valley floor, the same color differences appear to reflect differential development controlled in part by depth to the water table instead of age.

Shade / Shadow

Much of the variance in TM images is caused by topographic shading and shadows. This variance is shown in the $(1 - F_{shade})$ image [Fig. 4a)], which to first approximation depicts topography (see Adams et al., 1986). In areas where the $(1 - F_{shade})$ image is not influenced by topographic shading, on the valley floor and on the bajadas, subtle effects of subpixel surface roughness and vegetation canopy architecture are revealed. For example, partially regenerated wildfire scars on the bajada appear slightly lighter than their surroundings, a consequence of decreased vegetation height and density, and hence shadow.

Because vegetation type, vigor, and cover all affect the amount of subpixel shading and shadow in the scene, F_{shade} can be used to help differentiate communities. Together, the $(1 - F_{shade})$ and VF_s images permit separation of communities on physiognomic criteria. For example, irrigated meadows and stands of cottonwood trees both have 100% cover and VF_s values of nearly unity and cannot be differentiated by VF_s alone. However, they can be differentiated by F_{shade} because irrigated agricultural and pasture areas with nearly complete (100%) herbaceous cover cast less shadow than cottonwood trees. Differentiation by F_{shade} alone is not always possible in hilly terrain, but this problem can be minimized if shading and shadowing caused by the topography is modeled using a digital terrain image and removed.

Vegetation

We find a single reference vegetation endmember for the bajada. A second one describes the riparian areas that are concentrated on the valley floor

(Fig. 3). The same two vegetation reference endmembers were found in both TM images, taken in winter and spring of different years. For the bajada, the reference endmember is *Artemisia tridentata*; for the riparian lands it is *Populus Fremontii*. Spectra were measured in the laboratory of samples having approximately the same proportions of green leaves, stems, and branches found in the field.

We regard the *Artemisia* reference spectrum as representative of a set of similar spectra of many species from the desert scrub communities where the green-leaf area comprises a small proportion of the total biomass. Although the spectrum of *Artemisia* is typical of the bajada vegetation, we caution that *Artemisia tridentata* cannot be identified from TM images. Similarly, the spectrum of *Populus* is a proxy for the spectra of several kinds of green vegetation that show little or no woody material.

Soils

The two soil reference endmember spectra used to compute fraction images [Fig. 4c), d)] were from the valley floor. The "tan" soil endmember (SCS soil unit 635; hereafter SCS 635) is an argixeroll from the valley floor near Independence. It was better developed than the "gray" soil endmember (SCS 600), a light-colored sandy torriorthent from the base of the alluvial fans. Alone, these two soil types are inadequate to characterize the diversity of soils, rocks, and boulders of Owens Valley. However, their spectra characterize the two broad classes of soils that can be distinguished with the six TM bands.

Spectral variation in soils is evident along north-south transects across the Sierra bajada. Patterns in the soil fraction images [Fig. 4c), d)] contrast with those of the vegetation fraction image [Fig. 4b)] in that they do not conform to elevation contours, but rather delineate individual alluvial fans and depositional units of different age within the fans. These patterns are consistent with previous conclusions that the soil spectra on the Sierra bajada express both the lithologic diversity of parent materials emanating from the Sierra Nevada and soil development (Gillespie, 1982; Gillespie et al., 1986).

Soil studies and field surveys confirm that on the alluvial fans the two soil-fraction images of Figures 4c), d) accurately depict younger (10–25 ka) and older soils (~ 200 ka), respectively (Burke et al., 1986; Gillespie et al., 1986; Turrin and Gillespie, 1986; J. Herrick, personal communication, 1988; K. Whipple, personal communication, 1988). The spectral differentiation of soil ages appears to be associated with the degree of iron oxidation and the development of clay or claylike films on sand grains exposed on the surface of the soil. The older soils, spectrally characterized on the fans by SCS 635, have more iron in the oxidized state, resulting in lower visible reflectance and a tan color. This contrasts with the younger, poorly developed gray soils that spectrally resemble SCS 600. The older soils also have thicker clay films which decrease reflectance in TM Band 7, beyond the range of human vision.

The interpretive model for the spectral variability of granitic Sierran soils is applicable to the east-side bajada only on fans containing mainly granitic gravels, and even it is open to doubt because the soils developing in the arid rain shadow are more calcic. Elsewhere on the eastern bajada, the parent material on the fans consists mainly of Paleozoic carbonate and other metamorphic rocks. Patterns on the eastern bajada in the tan soil fraction image [Fig. 4d)] emphasize these lithologic differences. In this image, carbonates are dark (low reflectances in Band 7) whereas the playas and other tan soils are light, because these areas spectrally resemble the tan soil endmember. Where the granitic Santa Rita Flat pluton crops out in the Inyo range northeast of Independence, unweathered outcrops spectrally resemble the gray soil endmember [Fig. 4c)].

Although some soils are spectrally distinct, others are not and for these it is necessary to rely on ancillary data such as location or morphology to aid in the interpretation of the soil fraction images. For example, we found that some light alkaline valley-floor soils and some young bajada soils could be confused; this was because vegetation mixed with the alkaline soils spectrally mimicked SCS 600 in the six TM bands, as did the young bajada soils. The alkaline soils are found only on the valley floor, and the bajada soils are found only on the fans; thus they are distinguished by their location. Similarly, the red hematitic basalt cinder cones spectrally mimic the "tan" soil endmember [Fig. 4d)], but these cinder cones may be distin-

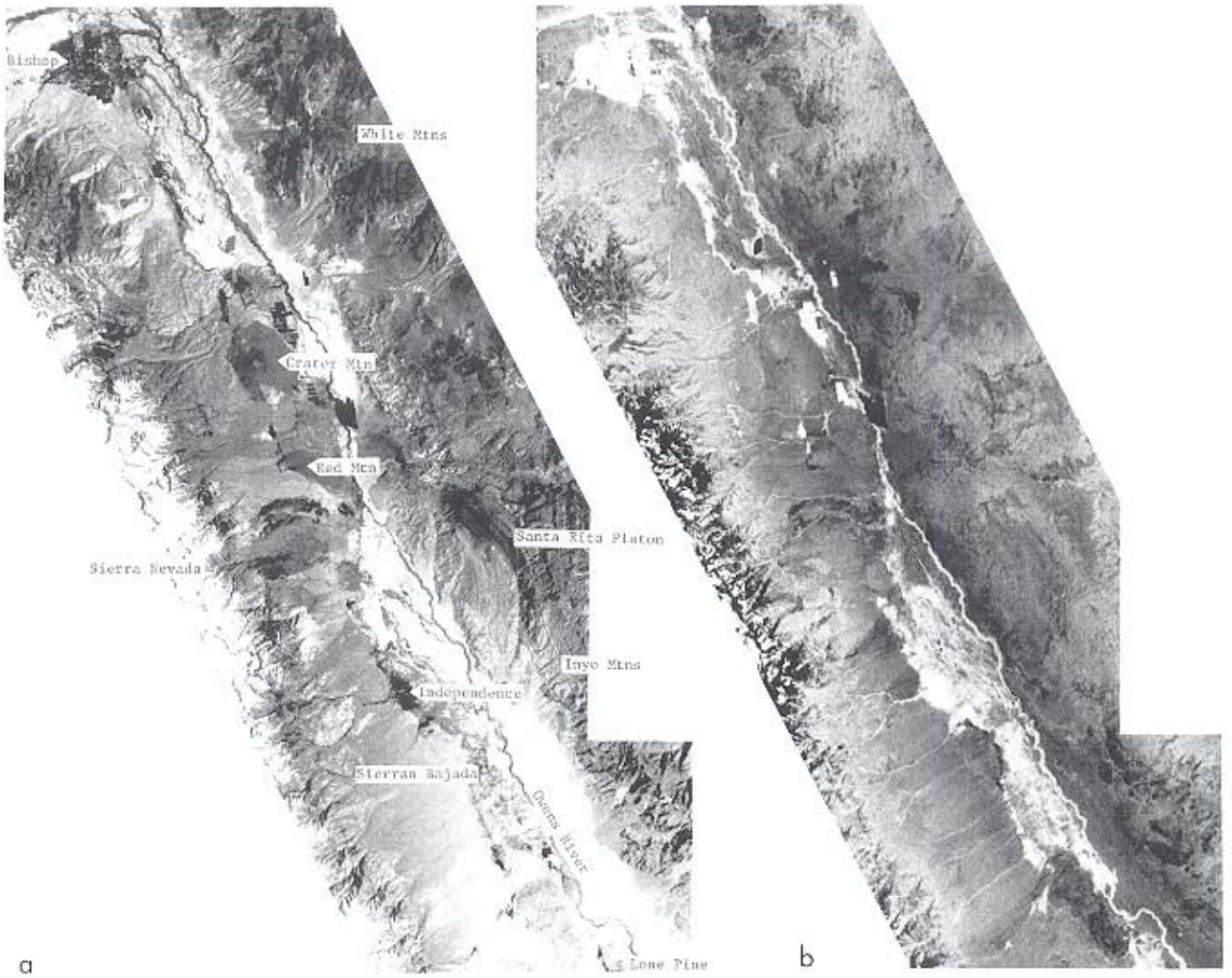

Figure 4. Fraction images of the reference endmembers, for the May TM image. Areas where the endmember comprises 100% of the spectral signature are white, whereas dark areas indicate the absence of the particular endmember. a) The complemented "shade" fraction image highlights steep topographical features due to changes in shadowing and surface orientation with respect to the solar illumination. High-albedo surfaces appear light in the image. b) The "vegetation" fraction (F_{veg}) image is marked by distinct areas of agriculture, irrigated pasture, and riparian areas. It illustrates the spatially continuous vegetation gradients on the bajadas as depicted in the contoured image of VF_s (Fig. 6), but differs in that the fraction of shade has not been removed by normalization using Eq. 3.

guished readily from the alluvium by their morphology.

Calibrating VF_s

Vegetation cover, as determined by field measurements, ranged from 0% to 100% for 112 map units covering 84,000 ha on the valley floor (unpublished data on file at the Bureau of Land Management and Inyo Country Water District, Bishop, CA). For the bajada, vegetation cover ranged from 0% to 50% for 31 transects and 11 plots covering areas the size of TM pixels (Ustin et al., 1986b; Teensma, 1981). Simple linear-regression analysis was used to determine the relationship between VF_s and the field measurements of vegetation cover for corresponding areas (Table 4).

Different results were obtained for the valley floor than for the bajada (Fig. 5). To quantify this difference, we computed separate regressions for the valley floor and bajada for each TM image. The same field data were used for each TM image. We also regressed VF_s values for the two different images. In each case linear regressions fit the data better than polynominal or other nonlinear regressions.

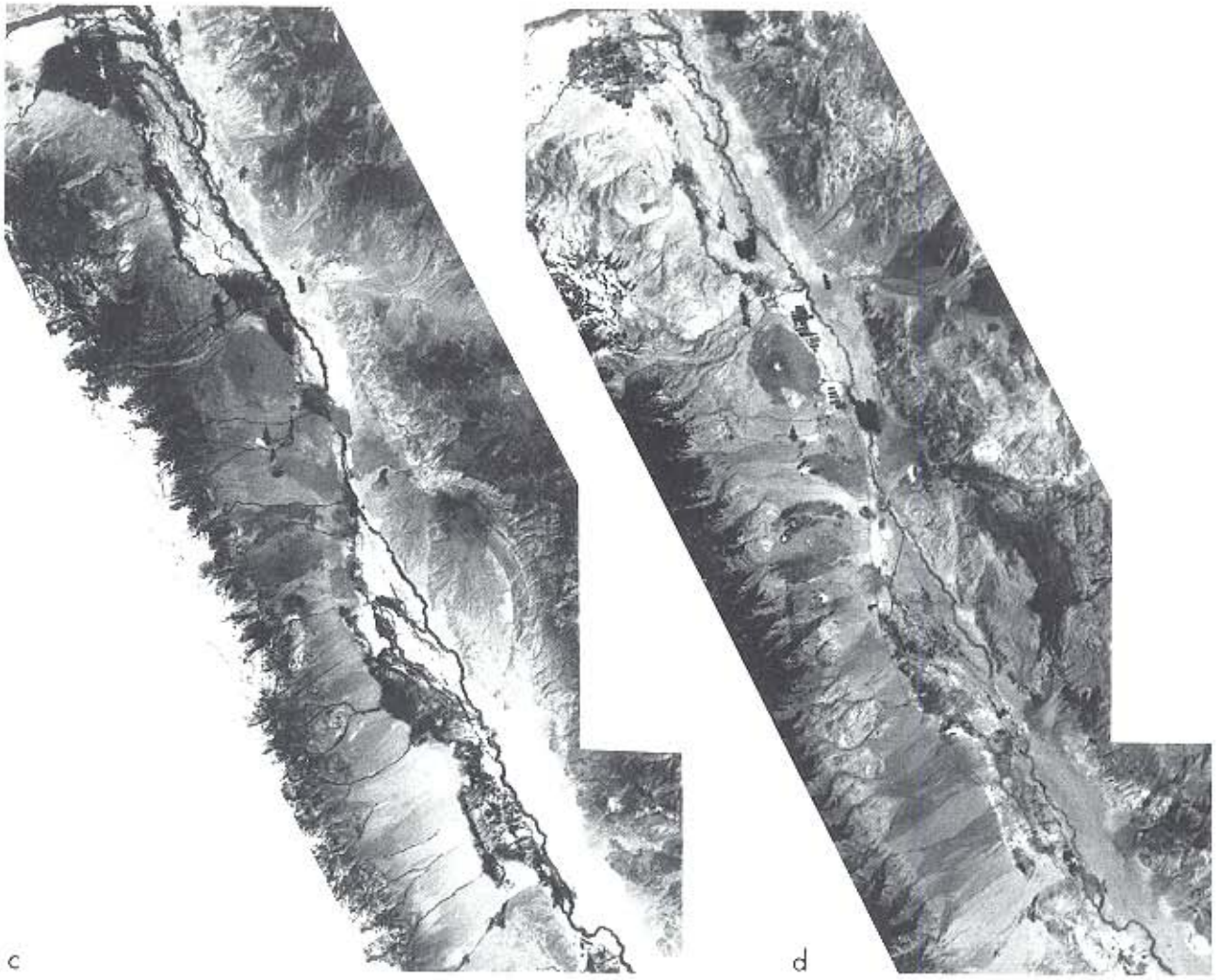

Figure 4 (cont.). Fraction images of the reference endmembers, for the May TM image. c) The "gray" soil (SCS 600) endmember is representative of young soils on the bajada and the highly alkaline soils of the valley floor. d) The "tan" soil endmember (SCS 635) corresponds both to older soils on the alluvial fans and to loamy valley-bottom soils, as well as to the red cinder cones.

Table 4. Linear Regression Models of Field Vegetation Cover Measurements vs. VF_v from Winter and Spring TM Images[a]

Regression	*Slope*	*Intercept*	*r*	*n*
y = cover fraction; $x = VF_v$				
Valley Floor (May image)	1.09	−0.02	0.84	112
Valley Floor (December image)	1.25	−0.05	0.80	112
Bajada (May image)	1.50	−0.04	0.91	42
Bajada (December image)	1.82	−0.02	0.87	42
y = May VF_v; x = December VF_v				
Valley Floor	1.21	−0.05	0.86	6000
Bajada	1.21	−0.03	0.95	10000

[a]Vegetation cover (%) was measured only once at each site during spring or summer. Here it is converted to cover fraction (0–1). The slopes of the regressed line (y = slope * x + intercept) are all > 1. The differences in regression slopes between seasons and between the valley floor and the bajada are consistent if VF_v corresponds to projected green-leaf area. Parameter r is the correlation coefficient and n is the number of data points.

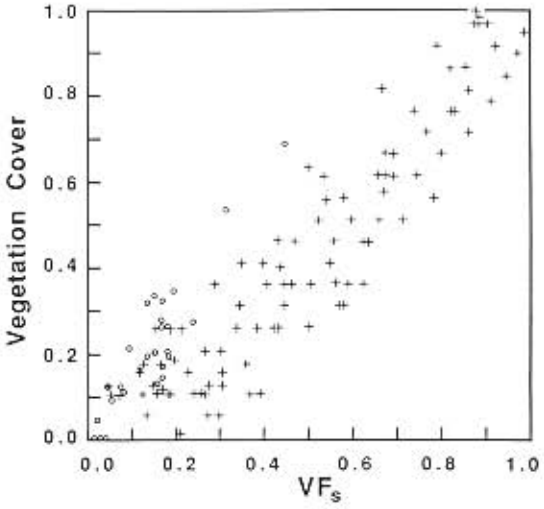

Figure 5. Comparison between vegetation cover measured in the field and calculated from the May vegetation fraction (VF_s), on the valley floor and on the alluvial fans. The differences in slope between the trends for the valley floor (+) and the bajada (○) indicate differences in the projected area of vegetation. The field measurements are always greater than the image estimates.

Although we obtained high correlations independent of season and location, the slopes of the regressed lines were different (Table 4). Regression slopes for both the valley floor and for the bajadas indicate that the vegetation fraction computed from ground measurements is greater than VF_s. In addition, the slope is consistently greater for the bajada vegetation than for vegetation on the valley floor, and greater in winter than in spring.

The regression slopes are greater than unity in Table 4 because the ground measurements of vegetation cover consistently overestimate the projected area of green leaves and woody biomass measured from above by the satellite. Thus, the ground measurements do not fully account for the gaps between the leaves and branches of the shrubs. The largest discrepancies occur for the shrubs characteristic of the lower bajada such as *Atriplex polycarpa*, *Grayia spinosa*, and *Tetradymia spinosa* which have comparatively low values (< 2) of leaf area index (LAI) and a low ratio of LAI to stem area or total biomass (Groeneveld et al., 1986b; Sorenson et al., 1988; Beatley, 1974; 1975; Chabot and Billings, 1972; Ustin et al., 1986a). Species such as *Purshia glandulosa* and *Artemisia tridentata* that are characteristic of the upper bajada have relatively high values of LAI, and a higher projected leaf area. Areas dominated by these shrubs have higher VF_s values that correlate more closely with the percent-cover measurements made on the ground.

Both the correlation coefficients and the slopes of the regression lines changed with season. The correlations between TM and ground measurements of vegetation differed between December and May. The December correlations are lower (Table 4) because the 23° sun elevation caused greater shadowing and lower spectral contrast. In May the sun elevation was 59°, resulting in less shadowing and more spectral contrast.

The regression slopes in Table 4 change with season, as is seen in the regression of VF_s values for the May image to those for the December image. This regresion slope exceeds unity for both the bajada and the valley floor, indicating consistently higher VF_s in spring vs. winter. This is consistent with increased amounts of projected green-leaf area in the spring due to new growth and, especially on the valley floor, to the appearance of ephemerals.

A picture of VF_s, coupled with $(1 - F_{shade})$ as discussed above, is given in Figure 6. The image has been color-coded and calibrated by field cover estimates so that the vegetation cover is ≤ 0.1 in gray areas, 0.11–0.3 in yellow areas, and > 0.30 in green areas. The color contours delineate vegetation patterns that for the most part are spatially continuous and lack abrupt transitions except for the riparian, irrigated and high-groundwater areas on the valley floor. Vegetation is more abundant on the west than on the drier east side of Owens Valley. Field transects show that the vegetation cover, and hence the LAI, increase with the elevation on the bajada on both sides of the valley.

The contours reveal a generalized correlation between elevation and bajada vegetation abundance, which is denser near the fan heads, and an asymmetry in cover due to decreasing precipitation and runoff with distance into the rain shadow toward the east. Vegetation cover is largely independent of soil type on the bajadas [Figs. 5 and 4c), d)]. This conclusion is supported by both the image data and field observations.

The E–W gradient in cover occurs across the transition in community from Great Basin Sagebrush on the west side to Mojave/Shadscale Scrub on the east side [Part II, Fig. 1b)]. The increase in cover occurs along with changes in community type. In general, the Mojave–Mixed Desert com-

Figure 6. A vegetation map of Owens Valley derived from multispectral TM images. The image has been color-coded and calibrated by field cover estimates so that the vegetation cover is ≤ 0.1 in gray areas, $0.11-0.3$ in yellow areas, and > 0.30 in green areas. The intensity of the color is modulated by $(1 - F_{\text{shade}})$. The Sierra Nevada on the left of the image is snow covered and the color codes are not applicable to this area.

munity occurs at low elevations and is found within the gray areas of Figure 6. The Great Basin Sagebrush community is found higher on the bajadas, in the yellow areas, and the Purshia–Piñon–Juniper communities occur at the fan heads and lower elevations of the montane regions, in the green zones. Exceptions to this overall pattern occur where the vegetation type changes from xerophytes to ephemerals or to phreatophytic communities, and where precipitation is anomalous (see Part II). For example, grasses are associated with the basalt flows, and mesic areas on the valley floor support phreatophytes [Fig. 4b)]. In contrast, areas of recent disturbance or of highly alkaline soils (e.g., salt pans) have unusually low vegetation fractions.

Cluster Analysis

Cluster analysis was performed on the measured and calculated variables listed in Table 5 to determine seasonal and spatial differences in image radiance data in relation to the computed fraction images and other remote-sensing measures of vegetation. We summarize the results of this analysis to illustrate that the radiance measurements alone do not consistently characterize the surface of Owens Valley either spatially or temporally.

Seasonal Differences and Internal Consistency

For each TM image there is a high degree of correlation among the six different radiance measurements (M1–5,7 and D1–5,7 in Table 5). In contrast, for most areas on the ground, radiance measurements were significantly different and were poorly correlated between the December and May images. These low correlations could be taken to imply intrinsic changes in the scene itself, or just changes in the illumination and instrument conditions extrinsic to the scene. It can be difficult to sort out these interpretations. The six bands of the TM images were all poorly correlated to the fraction images, with the single exception of the shade image.

The normalized soil reference endmember fractions of Table 5 were computed analogous to VF_s expressed by Eq. (3). Both the fractions for the December and May image utilized the same reference endmembers. The normalized soil and vegetation fractions (DTS, DGS, MTS, MGS; and DV, MV, respectively) computed for the December and May images were better correlated than the corresponding radiance images. Thus, unlike the images as acquired, the calculated fraction images provide a consistent framework or reference from which to evaluate temporal changes in the scene.

The shade fraction images from December and May [Fig. 4a)] were the least correlated of the four fraction images, because of the striking differences in shade and shadow in the scene that resulted from the greatly different summer and winter solar elevation angles. Temporal differences in band radiances corresponded predominantly to these same changes in shade and shadow. Although many changes in F_{shade} resulted from the large-scale topography, equally important changes resulted from shading and shadowing at subpixel scales.

Table 5. A Correlation Matrix of Radiances and Reference Endmember Fractions, Multiplied by 100, for December and May TM Images of Owe

	DTS	*MTS*	*MGS*	*M7*	*M5*	*M4*	*MSh*	*M3*	*M2*	*M1*	*D1*	*D2*	*D3*	*D4*	*DSh*	*D5*	*D7*	*DV*	*MV*	*MVI*	*DVI*	*I*
DGS	−89	−85	86	−27	−23	8	34	19	32	39	58	51	46	32	58	−23	−22	19	12	7	−21	
DTS		83	−80	32	28	−21	−7	−16	−23	−18	−36	−31	−31	−25	−51	29	39	−50	−29	−13	10	
MTS			−94	58	52	−1	−36	−3	−20	−30	−38	−29	−20	−8	−27	24	23	−36	20	1	−2	
MGS				−45	−41	6	−45	21	41	52	51	41	32	15	35	−16	−14	12	−40	−22	−11	
M7					97	83	74	79	76	75	17	32	40	43	30	63	61	−59	−79	7	5	
M5						86	75	77	75	76	20	35	44	46	35	65	62	−61	−75	17	16	
M4							90	85	86	81	43	55	58	57	54	60	57	−53	−69	12	32	
MSh								89	90	83	60	67	67	58	64	49	47	−54	−73	2	−12	
M3									93	83	53	62	66	56	58	55	54	−57	−78	−10	−9	
M2										92	64	67	68	53	60	48	49	−59	−77	−11	−8	
M1											69	69	66	49	60	42	42	−60	−77	−14	−10	
D1												82	84	83	84	74	74	−60	−63	−8	−23	
D2													87	86	84	80	81	−61	−68	−10	−16	
D3														88	87	85	85	−56	−71	−7	−8	
D4															90	84	85	−42	−73	−5	5	
DSh																79	77	−37	−66	1	4	
D5																	89	−53	−71	−13	12	
D7																		−68	−72	−16	4	
DV																			84	14	29	
MV																				23	32	
MVI																					38	
DVI																						
D43																						

Variable Abbreviation

Variable	*Description*	*Variable*	*Description*
M1	May TM Band 1	D1	Dec TM Band 1
M2	May TM Band 2	D2	Dec TM Band 2
M3	May TM Band 3	D3	Dec TM Band 3
M4	May TM Band 4	D4	Dec TM Band 4
M5	May TM Band 5	D5	Dec TM Band 5
M7	May TM Band 7	D6	Dec TM Band 6
MSh	May F_{shade}	DSh	Dec F_{shade}
MV	May VF_s	DV	Dec VF_s
MTS	May $F_{tan\ soil}/(1-F_{shade})$	DTS	Dec $F_{tan\ soil}/(1-F_{shade})$
MGS	May $F_{gray\ soil}/(1-F_{shade})$	DGS	Dec $F_{gray\ soil}/(1-F_{shade})$
MVI	May PVI	DVI	Dec PVI
M43	May VRI	D43	Dec VRI

VF_s: scaled vegetation fraction
PVI: perpendicular vegetation index
VRI: vegetation ratio index (TM Band 4/3 ratio)

The normalized vegetation fractions (DV, MV) changed from December to May. Although over the whole subscene DV and MV appear to be highly correlated, the actual relationship is not simple. For example, an area with a high VF_s in December will typically have a larger change between December and May than an area with a lower December VF_s. For an extreme example, dune fields on the floor of Owens Valley are sparsely vegetated in any season, and hence VF_s for these areas is unchanged.

The two normalized soil fractions at the different seasons (DTS vs. DGS and MTS vs. DGS) were found to be spatially correlated ($r < -0.89$). The correlation between the two soil fractions was more extreme than between soil and vegetation fractions. This difference is consistent with the insensitivity of the vegetation to edaphic differences as measured in the images. The inverse relationship between the normalized soil endmembers is one-to-one, indicating that they are spatially independent of both shade and vegetation. Patterns in images of the same soil endmember fractions for both December and May are consistent, such that the same soil map can be constructed from either TM image.

Other Vegetation Indices

Images of three conventional vegetation indices, VRI, NDVI, and PVI, were calculated from the two TM images, using only Bands 3 and 4 (Elvidge and Lyon, 1985). Index values for the valley floor and bajada were compared to field measurements of vegetation cover. On the valley floor, correlations between the index values and vegetation cover ranged from $r = 0.76$ to 0.83, for both December and May images. The correlations are not significantly different from those obtained for VF_s ($r = 0.80$ to 0.84; see Table 4). These uniformly high correlation coefficients result in part from the wide range of vegetation cover (0–100%). Among the three vegetation indices, PVI had the lowest correlation, for both May and December. There was little difference between values of r for NDVI and VRI.

On the bajada, correlations between the index values and vegetation cover differed from May to December. For the May image, $r = 0.32$–0.66; for the December image, $r = 0.33$–0.48. In contrast, for VF_s (May) $r = 0.91$; for VF_s (December) $r = 0.87$. As for the valley floor, of the three indices PVI had the lowest values of r, and NDVI and VRI were comparable.

A correlation matrix for two of the standard vegetation indices (VRI and PVI), VF_s and other parameters for the May and December images is given in Table 5. VRI, PVI, and VF_s, each a measure of vegetation, are inconsistent in the degree of correlation with other variables given in Table 5. The seasonal correlation of VF_s (MV vs. DV in Table 5) is relatively high compared to those for VRI or PVI (e.g., DVI or D43 vs. MVI or M43, respectively). None of the three indices correlates well with the normalized soil fractions. VRI has the highest correlation to the nominally calibrated image radiances (DN values).

DISCUSSION

The Physical Interpretation of Reference Endmembers

Finding a set of reference endmember spectra that fit the image data is part of the process of identifying the materials that actually comprise the scene. Equally important is the evaluation of the chosen reference endmembers to determine whether they are reasonable in light of other information about the field area, and whether their spectra are unique or merely representatives of broader classes.

The six-point spectra of TM rarely allow unique spectral identifications. For example, the reference "tan" soil is spectrally representative of a class of materials that includes the red hematitic basalt cinders (Table 3). However, TM spectra are adequate to identify some general spectral classes such as vegetation and certain types of soil and rock. Most of the materials in Owens Valley, when measured through TM bandpass filters, are spectrally indistinguishable from various mixtures of the reference endmembers, and vice versa. For example, a mixture of salt and sand (Table 3) appears similar to the "gray" soil spectrum, but is lighter (negative shade).

The spectrum of reference endmember *Artemisia* is similar to that of several other species of bajada vegetation. Thus, when a reference spectrum such as that of *Artemisia* is found to fit the image data, it is important to keep in mind that the search has only narrowed to an *Artemisia*-like material, not to a specific genus or species. Our

laboratory and field measurements of many plants indicate that few species have unique reflectance spectra. This is especially true using the restricted TM bandpasses. These conclusions are consistent with the fact that the spectral contrast responds primarily to the biochemical constituents (mainly chlorophyll and water) rather than to the morphology and physiognomy that are most often used to characterize plant species (e.g., Gates, 1970). However, the intensity (lightness) of spectra also responds to plant architecture (Adams and Smith, 1986), as is shown by the F_s image [Fig. 4a)].

Once the spectral class of the reference endmember has been established, it is possible to resolve ambiguities and to narrow the choices of reasonable materials further using additional knowledge of the field area. The spatial context of the endmember in the image is especially important. For example, we know that various evaporites (salts) occur on the valley floor and along the lower edges of fans. Salt rarely is mixed with other materials except along unit boundaries. Therefore, we exclude salt as an interpretation for the "gray" soil endmember on the bajadas.

The spectral ambiguity between dry grass and "tan" soil (Table 3) also can be resolved from the image context. In Owens Valley, we observe that fields of dry grass are found largely on the lower fans and valley floor. Spectrally, dry grass resembles mixtures of the "gray" and "tan" soil endmembers, which actually occur there also, but not together. Thus, we would interpret apparent spectral mixtures of "gray" and "tan" soil on the valley floor as representing actual mixtures of the "gray" soil plus dry grass and shrub litter, or alternatively as some mixture of the "tan" soil and other reference endmembers. The same data for the bajadas would be interpreted as a soil of intermediate development resembling a mixture of the endmember soils, because dry grass is uncommon there and a range of intermediate soils have been observed.

One further limitation to identifying materials in terms of spectral endmembers is the completeness of the collection of reference spectra that is used in the search. It is not feasible to collect the spectra of all possible materials. However, it is possible to assemble a set of spectra that includes the main materials that are known to occur in the field area or that are known to be reasonable candidates. These sets may comprise a few tens or a few hundreds of spectra. When the possible mixtures of all spectra are considered, these sets are seen to encompass a large range of spectral variation. Nevertheless, it is always necessary to keep in mind that unknown materials on the ground may masquerade as spectral mixtures of the reference endmembers that have been selected for the image.

The discovery of only two spectral vegetation endmembers among a diverse mix of plant species and community types—one for the mesic portions of the valley floor and one for the xeric bajada—conflicts with the results of many prior studies which conclude that multispectral images discriminate plant communities and/or species (e.g., Gross and Klemas, 1986; Satterwhite and Henley, 1987). The general correspondence between VF_s and community type in Owens Valley is not direct: It occurs only because there is a characteristic physiognomy, canopy architecture, and LAI for each community type, and not because the images measure vegetation community directly. Perhaps direct identification will be easier with the acquisition of very high spectral resolution (~10 nm) data by AVIRIS and related instruments that can record subtle spectral differences that characterize some species. However, studies that suggest that direct identification of desert vegetation can be made by TM (e.g., Satterwhite and Henley, 1987) are not consistent with our results.

Based on the correlations between the ground measurements of percent vegetation cover with VF_s, we conclude that VF_s is a quantitative measure of vegetation abundance. The differences between the vegetation reference endmembers for the bajada and the valley floor are consistent with differences in the amount of woody material exposed and in the projected green-leaf area. Similarly, the seasonal changes in the VF_s are consistent with measured seasonal changes in LAI (Groeneveld et al., 1986b; 1987).

It was not possible to regard the ground measurements as an absolute reference against which the accuracy of VF_s could be judged. Despite careful field work by different experienced botanists, ground measurements overestimated the shrub cover because it was not feasible to measure the many small gaps between the leaves and branches. We suggest that VF_s actually may give a more accurate instantaneous measure of projected vegetation cover than one-time ground measure-

ments; however, to test this possibility, it would be necessary to make exceptionally detailed ground measurements during TM image acquisition. This work has not been attempted.

The Correspondence between VF_s and Other Indices

Estimates of vegetation abundance from VF_s and three conventional indices (PVI, NDVI, and VRI) were different for the Owens Valley study area (Ustin et al., 1986a; Smith et al., 1988b). For riparian areas, PVI, NDVI, and VRI and VF_s correlated well with field measurements, although the standard indices all indicated higher cover in December than May—contrary to field observations. For desert scrub, the standard indices were less well correlated than VF_s to field measurements. This suggests that PVI, NDVI, and VRI are not sensitive to the subtle variations of vegetation abundance typical of arid and semiarid regions. Again, PVI, NDVI, and VRI all were greater for the winter than for the spring image. Interpretation of each measure of vegetation leads to different conclusions regarding seasonal changes in the vegetation and its spatial distribution.

We attribute to the assumptions implicit in these indices the lack of correlation between PVI, NDVI, and VRI and field vegetation measurements. These indices use only two spectral bands to determine the relative abundance of vegetation. Theoretically, it is not possible to resolve more than three spectral endmembers using only two spectral bands. However, for Owens Valley we found five distinct endmembers using TM. Thus, when only two bands are used to determine vegetation abundance it is not possible to entirely remove the spectral contributions from the other endmembers. For this reason, VRI and PVI may yield incorrect abundance estimates when used on multispectral images that have more than a single soil or vegetation endmember, as has been demonstrated by Elvidge and Lyon (1985), Huete (1986), and Huete et al. (1985). Even the six TM bands are not fully adequate to separate all of the Owens Valley soils and vegetation, as is evidenced by the negative fractions in Table 3. New high spectral resolution scanners such as the 224-band AVIRIS may eventually be capable of differentiating more endmembers than TM in the Owens Valley; however, preliminary application of spectral mixture analysis to AVIRIS (Smith et al., 1988a) resulted in the same number of endmembers, which we suspect may be intrinsic to the scene.

From Table 5 it is possible to predict the outcome of supervised and unsupervised classification schemes such as maximum likelihood, discriminant analysis, *K*-mean clusters, principal components analysis, etc., applied to the radiance data. Each of these analytical frameworks relies on the statistical distributions of the different bands of radiance data to delineate different surface types in the image and to permit the inference of surface composition. Any classification scheme that cannot separate the influence of shading and shadow from soil and vegetation in an image will incorporate some unknown weighting of mixtures from these components which depends upon the imaged scene. Because shading and shadow often exert the greatest influence on spectral variation in the acquired image, statistical schemes of classification necessarily incorporate these variable components as part of the classification. The statistical classification gives inconsistent results from images acquired for the same area at different seasons because the shading and shadow change, corresponding to the conditions of the respective solar elevation and azimuth angles.

SUMMARY AND CONCLUSIONS

Using spectral mixture analysis on TM images of Owens Valley, we separated the vegetation from the other surface components and from the effects of differential illumination, atmosphere, and instruments response. Seasonal changes in vegetation on the bajada and valley floor are expressed spectrally in the TM images as changes in the endmember fractions. The vegetation endmember spectra themselves did not change from winter to spring, although the fraction of vegetation did increase. The spatial patterns of the two soils, independent of the vegetation and shade spectral components, were equivalent for the December and May images, despite a large difference in sun elevation and differences in the fraction of vegetation. The endmembers found in the Owens Valley appear to be representative of the broad types of vegetation and rock/soil found elsewhere in the Great Basin and Mojave Deserts, suggesting that

the results of this study may be extended to other similar regions.

The results of this study emphasize that the vegetation abundance must be measured in context with all of the other factors that influence the spectral variation in multispectral images. Many remote sensing studies are focused narrowly on single factors such as vegetation, on the assumption that other factors such as the soils and the lighting conditions can be ignored. Our experience suggests that this limited focus can result in misinterpretation of the spectral content of images.

We have found that standard field techniques as applied to desert scrub do not yield a sufficiently accurate measure of the vegetation as projected onto the image plane, yet it is this measure that is required to link field and remote observations. A simple and effective field technique is required to measure the projected area of leaves and woody material, possibly utilizing the new generation of compact and portable multispectral CCD cameras.

Once the spectral endmembers are determined for an area, they form the basis for calibrating subsequent images, according to Eq. (2). The spectral mixture analysis then can be used to monitor changes in the fractions of endmembers, such as vegetation, with season and with changes in land use. If the endmembers themselves change this will be apparent in the fit of the model to data. We conclude, therefore, that the approach is advantageous for ecological, land-use, and other studies of changes in vegetation where it is important not to have confusion with variations in lighting, atmospheric, and instrumental effects.

We acknowledge the assistance of the staff and the use of facilities at the University of California White Mountain Research Station. We thank P. Novak and the Los Angeles Department of Water and Power for providing us with a vegetation map of the Independence Quadrangle, A. F. Fischer III and the Soil Conservation Service for sharing their knowledge of Owens Valley soils, and R. A. Woodward for assistance in sampling vegetation. We thank S. Willis, P. Shippert, and D. Nitsch for support with image analysis and manuscript preparation, and G. Bradshaw for critical reviews. Thanks to G. Vogler for layout and final presentation of graphics and images. We thank J. Herrick and K. Whipple for discussions of their ongoing research and permission to quote their tentative results. This research was partially supported by NASA Grant NAS7-918 and Jet Propulsion Laboratory Subcontract 956899, and NASA Grants NASW 4016 and NASW85 to the University of Washington. We gratefully acknowledge the W. M. Keck Foundation for computer equipment and support.

REFERENCES

Adams, J. B., and Adams, J. (1984), Geologic mapping using LANDSAT MSS and TM images: Removing vegetation by modeling spectral mixtures, in *Third Thematic Conf. Remote Sensing for Expl. Geol.*, ERIM, Colorado Springs, CO, Vol. 2; pp. 615–622.

Adams, J. B., and Smith, M. O. (1986), Architecture: Shade and shadow in geobotanical mapping (abs.), in *Fifth Thematic Conf., Remote Sensing for Expl. Geol.*, ERIM, Houston, TX, Vol. 111.

Adams, J. B., Smith, M. O., and Johnson P. E. (1986), Spectral mixture modeling: a new analysis of rock and soil types at the Viking Lander 1 Site, *J. Geophys. Res.* 91:8098–8112.

Adams, J. B., Smith, M. O., and Gillespie, A. R. (1989), Simple models for complex natural surfaces: a strategy for the hyperspectral era of remote sensing, in *Proc. IEEE Int. Geosci. and Remote Sensing Symp. '89 I*, IEEE, New York, pp. 16–21.

Anuta, P., Bartolucci, L., Dean, M., Lozano, D., Malaret, E., McGillem, C., Valdes, J., and Valenzuela, C. (1984), Landsat-4 MSS and Thematic Mapper data quality and information content analysis, *IEEE Trans. Geosci. Remote Sens.* (3) GE-22:222–236.

Barker, J. (1983), Radiometric calibration and processing procedures for reflective bands on Landsat-4 protoflight, in *Proc. Landsat-4 Scientific Characterization Early Results Symposium*, A-23-1, NASA/GSFC, Greenbelt MD.

Beatley, J. C. (1974), Effects of rainfall and temperature on the distribution and behavior of *Larrea tridentata* (Creosote-Bush) in the Mojave desert of Nevada, *Ecology* 55:245–261.

Beatley, J. C. (1975), Climate and vegetation patterns across the Mojave/Great Basin transition of southern Nevada, *Am. Midl. Nat.* 93:53–70.

Billings, W. D. (1945), Plant associations of the Carson Desert region, Western Nevada, *Butler Univ. Bot. Stud.* 7:89–123.

Billings, W. D. (1949), The shadscale vegetation zone of Nevada and Eastern California in relation to climate and soils, *Am. Midl. Nat.* 42:87–109.

Burke, R. M., Lunstrom, S., Harden, J., Gillespie, A. R., and Berry, M. (1986), Soil chronosequence on eastern Sierra Nevada fans, CA, supports remote sensing studies, *Geol. Soc. Am. Abstr. Program* (6) 8:553.

Chabot, B. F., and Billings, W. D. (1972), Origins and ecology of the Sierra Alpine flora and vegetation, *Ecol. Mono.* 42:163–199.

Choudhury, B. J. (1988), Relationships between vegetation indices, radiation, absorption, and photosynthesis evaluated by a sensitivity analysis, *Remote Sens. Environ.* 22:209–233.

Conel, J. E., and Alley, R. E. (1984), Lisbon Valley, Utah, uranium test site report, in *The Joint NASA / Geosat Test Case Project Final Report*, (Paley, H. N., Ed.), AAPG Bookstore, Tulsa, OK, Part 2, Vol. 1, Sec. 8; pp. 1–101.

Crist, E. P., and Cicone, R. C. (1984), A physically-based transformation of Thematic Mapper data—the TM tasseled cap, *IEEE Trans. Geosci. Remote Sens.*, (3) GE-22:256–263.

Dixon, W. J., Brown, M. B., Engelman, L., Frane, J. W., and Jennrich, R. I., Eds. (1979), BMDP-79: Biomedical Computer Programs, P-Series, University of California Press, Berkeley.

Elvidge, C. D., and Lyon R. J. P. (1985), Influences of rock and soil spectral variation on the assessment of green biomass, *Remote Sens. Environ.* 17:265–279.

Gates, D. M. (1970), Physical and physiological properties of plants. Remote Sensing with special references to agriculture and forestry, *Nat. Acad. Sci. USA*: 224–252.

Gillespie, A. R. (1982), Quaternary glaciation and tectonism in the southeastern Sierra Nevada, Inyo County, California, Ph.D. thesis, Caltech, Pasadena, CA, 695 pp.

Gillespie, A. R., Abbott, E. A., and Hoover, G. (1986), Spectral basis for relative dating of granitic alluvial fans, Owens Valley, CA (abs.), *Geol. Soc. Am.* 18:614.

Goetz, A. F. H., Billingsley, F. C., Gillespie, A. R., Abrams, M. J., Squires, R. L., Shoemaker, E. M., Lucchitta, I., and Elston, D. P. (1975), Application of ERTS images and image processing to regional geologic problems and geologic mapping in northern Arizona, NASA-JPL 32-1597, JPL, Pasadena, CA.

Gradie, J., and Veverka, J. (1982), When are spectral curves comparable?, *Icarus* 49:109–119.

Greegor, D. H. J. (1986), Ecology from space, *BioScience* 35:429–432.

Griepentrog, T. E., and Groeneveld, D. P. (1981), The Owens Valley Water Management Report, Inyo County, Bishop, CA, 273 pp.

Groeneveld, D. P., Elvidge, C. D., and Monat, D. A. (1986a), Hydrologic alteration and associated vegetation changes in the Owens Valley, CA, in *Proc. Arid Lands Today and Tomorrow: Int. Arid Lands Res. and Dev. Conf.*, Univ. of Arizona Press, Tucson, pp. 1373–1382.

Groeneveld, D. P., Warren, D. C., Hubbard, P. J., and Yamashita, I. S. (1986b), Transpiration processes of shallow groundwater shrubs and grasses in the Owens Valley, CA. Phase #1: Steady state conditions, Inyo County, Bishop, CA, 130 pp.

Groeneveld, D. P., Warren, D. C., and Rawson, R. H. (1987), Estimation of evapotranspiration by percent plant cover for the western Great Basin, *EOS Trans. Am. Geophys. Union* 68:1299.

Gross, M. F., and Klemas, V. (1986), The use of airborne imaging spectrometer (AIS) data to differentiate marsh vegetation, *Remote Sens. Environ.* 19:97–103.

Hapke, B. (1981), Bidirectional reflectance spectroscopy: I. Theory, *J. Geophys. Res.* 86:3030–3054.

Haralick, R. M., and Fu, K. S. (1983), Pattern recognition and classification, in *Manual of Remote Sensing*, 2nd ed. (R. N. Cowell, Ed.), Am. Soc. Photogramm., Falls Church, VA, Vol. 2, pp. 793–806.

Heilman, J. L., and Boyd, W. E. (1986), Soil background effects on the spectral response of a three-component rangeland scene, *Remote Sens. Environ.* 19:127–137.

Hollett, K. J., Danskin, W. R., McCaffrey, W. F., and Walti, C. L. (1988), Hydrogeology and water resources of Owens Valley, California, U.S.G.S. Water-Supply Paper 2370-B, 118 pp.

Horwitz, H. M., Lewis, J. T., and Pentland, A. P. (1975), Estimating proportions of objects from multispectral scanner data, Final Report, NASA Contract NAS9-14123, NASA-CR-141862, 108 pp.

Huete, A. R. (1986), Separation of soil-plant spectral mixtures by factor analysis, *Remote Sens. Environ.* 19:237–251.

Huete, A. R., Post, D. F., and Jackson, R. D. (1984), Soil spectral effects on 4-space vegetation discrimination, *Remote Sens. Environ.* 15:155–165.

Huete, A. R., Jackson, R. D., and Post, D. F. (1985), Spectral response of a plant canopy with different soil backgrounds, *Remote Sens. Environ.* 17:37–53.

Jackson, R. D. (1983), Spectral indices in *n*-space, *Remote Sens. Environ.* 14:409–421.

Johnson, P. E., Smith, M. O., Tayor-George, S., and Adams, J. B. (1983), A semiempirical method for analysis of the reflectance spectra of binary mineral mixtures, *J. Geophys. Res.* 88:3557–3561.

Justice, C. O., Townshend, J. R. G., Holben, B. N., and Tucker, C. J. (1985), Analysis of the phenology of global vegetation using meteorological satellite data, *Int. J. Remote Sens.* 6:1271–1318.

Kauth, R. I., and Thomas, G. S. (1976), The tasselled cap—a graphic description of the spectral temporal development of agricultural crops as seen by Landsat, in *Proc. 3rd Symp. Machine Processing of Remotely Sens. Data*, LARS, Purdue Univ., W. Lafayette, IN, pp. 4B/41–4B/51.

Kearney, T. H., Briggs, L. J., Shantz, H. L., McLane, J. W., and Piemeisel, R. L. (1914), Indicator significance of vegetation in Toole Valley, Utah, *J. Agri. Res.* 1:365–417.

MacMahon, J. A., and Wagner, F. H. (1985), The Mohave, Sonoran, and Chihuahuan Deserts of North America, in *Hot Deserts and Arid Shrublands, Ecosystems of the World* (M. Evenari and I. Noy-Meir, Eds.), Elsevier, Amsterdam, Vol. 12, pp. 105–202.

NOAA (1986), Climatological Data Annual Summary, California, Vol. 90.

Odum, E. (1983), *Basic Ecology*, Saunders College Publishing, San Francisco, 613 pp.

Otterman, J., Ungar, S., Kaufman, Y., and Podolak, M. (1980), Atmospheric effects on radiometric imaging from satellites under low optical thickness conditions, *Remote Sens. Environ.* 9:115–129.

Pech, R. P., Graetz, R. D., and Davis, A. W. (1986), Reflectance modelling and the derivation of vegetation indices for an Australian semi-arid shrubland, *Int. J. Remote Sens.* 7:389–403.

Possolo, A., Adams, J. B., and Smith, M. O. (1990), Mixture models for multispectral images, *J. Geophys. Res.*, forthcoming.

Richardson, A. J., and Wiegand, C. L. (1977), Distinguishing vegetation from soil background information, *Photogramm. Eng. Remote Sens.* 43:1541–1552.

Robinove, C. J. (1982), Computation with physical values from Landsat digital data, *Photogramm. Eng. Remote Sens.* 48:781–784.

Satterwhite, M. B., and Henley, P. J. (1987), Spectral characteristics of selected soils and vegetation in northern Nevada and their discrimination using band ratio techniques, *Remote Sens. Environ.* 23:155–175.

Shantz, H. L., and Piemeisel, R. L. (1940), Types of vegetation in Escalante Valley, Utah, as indicators of soil conditions, USDA Tech. Bull. 713, 46 pp.

Shipman, H., and Adams, J. B. (1987), Detectability of minerals on desert alluvial fans using reflectance spectra, *J. Geophys. Res.* 92:10391–10402.

Smith, M. O., Johnson, P. E., and Adams, J. B. (1985), Quantitative determination of mineral types and abundances from reflectance spectra using principal components analysis, in *Proc. 15th Lunar Planet. Sci. Conf.*, J. Geophys. Res., 80 Suppl., Part 2, pp. C797–C804.

Smith, M. O., Adams, J. B., and Gillespie, A. R. (1988a), Evaluation and calibration of AVIRIS test-flight data: Owens Valley, CA, Final Report NASA Contract No. NAGW 1135, 17 pp.

Smith, M. O., Adams, J. B., and Roberts, D. A. (1988b), Removing the spectral effects of vegetation in multispectral images (abs), in *Proc. 22nd Int. Symp. Remote Sens. Environ., 7th Thematic Conf: Remote Sensing for Exploration Geology*, ERIM, Houston, TX.

Smith, M. O., Ustin, S. L., Adams, J. B., and Gillespie, A. R. (1990), Vegetation in deserts: II. Environmental influences on regional abundance, *Remote Sens. Environ.*, this issue.

Sorenson, S. K., Dileanis, P. D., and Branson, F. A. (1988), Vegetation and soil water responses to changes in precipitation and depth to ground water in Owens Valley, CA, USGS water supply report, forthcoming.

Teensma, P. D. A. (1981), Sagebrush (*Artemisia tridentata* Nutt.) and fire in Owens Valley, California, M.A. thesis, University of Oregon, Eugene OR, 74 pp.

Tucker, C. J. (1979), Red and photographic infrared linear combinations for monitoring vegetation, *Remote Sens. Environ.* 8:127–150.

Tucker, C. J., and Miller, L. D., (1977), Soil spectra contributions to grass canopy spectral reflectance, *Photogramm. Eng. Remote Sens.* 43:721–726.

Tucker, C. J., Hielkema, J. C., and Roffey, J. (1985), Satellite remote sensing monitoring in desert locust breeding areas, *Int. J. Remote Sens.* 6:127–138.

Tucker, C. J., Fung, I. Y., Keeling, C. D., and Gammon, R. H. (1986), Relationship between atmospheric CO_2 variations and a satellite-derived vegetation index, *Nature* 319: 195–199.

Tueller, P. T., and Oleson, S. G. (1989), Diurnal radiance and shadow fluctuations in a cold desert shrub plant community, *Remote Sens. Environ.* 29:1–13.

Turrin, B., and Gillespie, A. R. (1986), K/Ar ages of basaltic volcanism of the Big Pine volcanic field, California: Implications for glacial stratigraphy and neotectonics of the Sierra Nevada (abs.), *Geol. Soc. Am.* 18:777.

USGS (1979), *Landsat Data User's Handbook*, rev. ed., USGS Branch of Distribution, Arlington, VA.

Ustin, S. L., Adams, J. B., Elvidge, C. D., Rejmanek, M., Rock, B. N., Smith, M. O., Thomas, R. W., and Woodward, R. A. (1986a), Thematic mapper studies of semi-arid shrub communities, *BioScience* 36:446–452.

Ustin, S. L., Rock, B. N., and Woodward, R. A. (1986b), Use of remote sensing techniques in the analysis of semi-arid shrub communities, in *Proc. White Mountain Research Station High-Altitude Symposium*, White Mountain Research Station, University of California, Los Angeles, pp. 84–98.

Walter, H. (1979), *Vegetation of the Earth and Ecological Systems of the Geo-Biosphere*, 2nd ed. (J. Wieser, Trans.), Springer-Verlag, New York, 274 pp.

Waring, R. H., Aber, J. D., Melillo, J. M., and Moore, B., III (1986), Precursors of change in terrestrial ecosystems, *BioScience* 36:433–438.

West, N. E. (1983a), Overview of North American temperate deserts and semi-deserts, in *Temperate Deserts and Semi-Deserts* (N. E. West, Ed.), Elsevier, Amsterdam, pp. 321–330.

West, N. E. (1983b), Great Basin-Colorado plateau sagebrush semi-desert, in *Temperate Desert and Semi-Deserts* (N. E. West, Ed.), Elsevier, Amsterdam, pp. 331–350.

West, N. E. (1983c), Colorado Plateau-Mojavian Blackbrush semi-desert, in *Temperate Deserts and Semi-Deserts* (N. E. West, Ed.), Elsevier, Amsterdam, pp. 399–411.